Louisiana State University
LSU Digital Commons

LSU Master's Theses | Graduate School

2005

Fracture behavior of wood plastic composite (WPC)

Gi Young Jeong
Louisiana State University and Agricultural and Mechanical College

Follow this and additional works at: https://digitalcommons.lsu.edu/gradschool_theses

 Part of the Environmental Sciences Commons

Recommended Citation

Jeong, Gi Young, "Fracture behavior of wood plastic composite (WPC)" (2005). *LSU Master's Theses*. 3397.
https://digitalcommons.lsu.edu/gradschool_theses/3397

This Thesis is brought to you for free and open access by the Graduate School at LSU Digital Commons. It has been accepted for inclusion in LSU Master's Theses by an authorized graduate school editor of LSU Digital Commons. For more information, please contact gradetd@lsu.edu.

FRACTURE BEHAVIOR OF WOOD PLASTIC COMPOSITE (WPC)

A Thesis
Submitted to the Graduate School of the
Louisiana State University and
Agricultural and Mechanical College
in Partial Fulfillment of the
Requirements for the Degree of
Master of Science
in
The School of Renewable Natural Resources

by
Gi Young Jeong
B.S., Chonnam National University, 2004
August, 2005

ACKNOWLEDGEMENTS

First of all, I would like to express my appreciation to my advisor Dr. Qinglin Wu for his advice and patience during my master courses. Dr. Wu let me forge my own path in formulating my research problems. I possessed more freedom and at the same time, more responsibility than other graduate students. I am very grateful for the opportunities afforded to me.

I would like to thank my committee: Dr. W. Ramsay Smith and Dr. Kun Lian for their time and comments in preparing this thesis. I would also like to extend a special thank to Dr. Lu. He provided much insight, advice, and friendship over the years that I worked in the same laboratory. I would also like to thank Dr. Sincliar. He helped me get familiar with the concept of finite element analysis. We discussed the problems related to my research. All of the above proved to be valuable mentors in the pursuit of my master degree.

Last but not least I would like to give my respect to my parents. They have always had faith in me and what I was doing even when I had lost it. Thank you for your unconditional love and sacrifice. They are the most important part of my life. I also want to say thank you to my friends: Byung Hyn, Gwang Su, Jong Sik, Ji Hun, and Ji Young. You guys are awesome. I am really lucky to have you guys as my buddies.

TABLE OF CONTENTS

LIST OF TABLES

LIST OF FIGURES

ABSTRACT

In this study, the effect of notch length on impact strength and fracture toughness was examined to exploit the use of wood plastic composite (WPC) as structural materials. Impact and fracture toughness test methods and estimation procedures were carried out. To evaluate the impact strength of WPC, five different notch sizes with two different fiber orientations on the load head were prepared. In terms of fracture mechanics, notch length was converted to stress concentration factor and the relationship between stress concentration factor and impact strength was determined. Fracture surface of impact specimens was investigated to evaluate the fracture mechanism of WPC by scanning electron microscopy (SEM). For the determination of fracture toughness of WPC, a short bar specimen with a rectangular cross section and a different notch size was used. To obtain the stress intensity factor (K_I) for the mode I case, a finite element method (FEM) was carried out. The simulation of the stress intensity factor was performed on four successively refined meshes via quarter point elements around the crack tip. By means of an asymptotic analysis, the verification of the simulation was also presented. The experimental results showed that impact strength of WPC was highly dependant upon the fiber orientation and stress concentration factor. However, fracture toughness was independent of the change of the length of the notch. Fracture toughness of WPC was estimated to be 1.79 MPa$\sqrt{m}$ using a four point bending test. The results of the simulation showed that stress intensity factor of WPC was estimated to be 584.9 (kPa$\sqrt{m}$). The results of normal stress at the crack tip from a common sequence of four successively refined meshes were diverged while the results of the stress intensity factors

converged. The strength of singularity for normal stress (σ_x) was 4.92 which is quite close to that of true singularity (0.5) for the sharp crack tip when Θ=180°. Crack opening angle (COA) of the four point bending specimen was also estimated to be 50° on the basis of strength of singularity determined from finite element method.

CHAPTER 1. INTRODUCTION

1.1 DEVLOPMENT AND HISTORY OF WOOD PLASTIC COMPOSITE (WPC)

The rapidly changing economic and environmental needs of society are putting ever increasing pressures on the forestry industry to do more with less. In practical terms, this means, for example, increasing conversion and efficient use of wood fiber resources, producing more fiber on a shrinking land base, using environmentally friendly processes and technologies, and remaining competitive in the global market place. Within the next decade, composites are expected to constitute the most prominent segment of the board industry. Competition in high volume markets has focused attention on low priced materials that offer a more favorable strength to weight ratio. Compared to other polymeric materials, wood plastic composite (WPC) has the lowest material cost. Wood plastic composites are an attractive alternative because their manufacturing process is highly automated and adaptable to various species and forms of raw materials. Sometimes wood is not considered as an engineering material because it does not have consistent, predictable, reproducible, continuous, and uniform properties. This might be true for solid wood but is not necessarily true for composites made from wood (Rowell *et al*., 1993). Wood flour has been used as filler in synthetic plastics (primarily thermosetting polymers) for decades. The use of wood in thermoplastics is a relatively recent phenomenon spurred by improvements in processing technology, development of suitable chemical coupling agents and economic factors. Advantages such as reductions in operating temperatures, cycle times, and mold shrinkage have also been instrumental in the growth of the fiber/plastic composite industry. The importance and growing

potential of wood plastic composites were evidenced in 1991 by the advent of the international conference on wood fiber-plastic composites, a forum on the science and technology for the processing and development of these materials (Smith 2001).

The consulting firm of Kline&Company (Little Falls, New Jersey) recently conducted an extensive market survey regarding the fiber/plastic composite industry. The use of fillers by the plastic industry has grown steadily along with the growth in the production of major classes of plastic resins. In 1967, the U.S. demand for fillers by the plastic industry was 525,000 tons; filler use had grown to 1,925,000 tons by 1998 (Eckert 1999). The projected use of fillers by the U.S. plastic industry in 2000 swelled to 5.5 billion pounds, of which 0.4 billion pounds (7%) was estimated to be bio-based fibers (Eckert 2000). Most bio-fiber plastic additives are derived from wood. However, other natural fibers, such as flax or wheat straw are finding their way into the fiber/plastic industry. Although calcium carbonate constitutes the major filler used by weight (66%), it accounted for only 32% ($140 million) of the total value of fillers used in 1998 ($435 million total). Other fillers, including natural fibers, command higher prices than calcium carbonate. Eckert (2000) reported average per pound prices of commonly used plastic fillers as follows: fiberglass, $0.90, natural fibers other than wood, $0.20, wood fiber, $0.10, and calcium carbonate, $0.70. Eckert (2000) also summarized major markets for natural fibers in plastic composites as follows, on a weight basis: building products, 70%; other (including marine uses, infrastructure), 13%; industrial consumer, 10%; and automotive, 7%. Although the U.S. annual growth in plastic demand is forecast at approximately 4.5% per year for 1998-2005, substantially greater growth in the demand for natural fibers is expected. This includes a rate in excess of 50% per year for the

period 2000-2005 in the building products area; a significant portion of this growth will be attributed to larger market share for fiber/plastic lumber in residual decking (Smith *et al*., 2001). A smaller, but significant subset of the building products market is also found in vinyl windows (Cannon, 1999). Wood fiber, at weight loading up to 70%, is used in vinyl or vinyl-clad wood window components. The wood materials and engineering laboratory at Washington State University has directed an interdisciplinary and inter-institutional research program for the development of HDPE (high density polyethylene)- and PVC-wood composite materials for use in waterfront structures. A major research and development effort is centered around waterfront applications for Navy facilities (Smith 2001). WPC is being investigated to replace treated timber currently used to support piers and absorb the shock of docking ships. The material development component of the Navy project is focusing on evaluation and improvement of existing wood-plastic composite technologies as well as developing novel systems appropriate to the production of pier structural components (Wolcott, 2000). Reinforcement of wood-plastic composites with carbon fibers was examined, but problems were encountered with PVC prepregs because of thermal degradation. Material structural studies revealed a large degree of processing-induced damage in the wood particles in PVC formulations as evidenced by reduced particle size. Co-extrusion of PVC WPC formulations with caps was successful. However, formulations were restricted to light color compounds. The PVC formulations were found to be viable for use in industrial deckboards. Natural fiber use in automotive fiber/plastic applications has been increased by 15% per year during 2000-2005. To date, most natural fiber/plastic materials in the automotive area have been HDPE or PP blends. While there is substantial growth in this area in North America,

Europe appears to lead the way in the use of wood-plastic composites for automobiles. These examples serve to illustrate the growing levels of interest in wood-plastic composites from both research and commercial standpoints.

1.2 BRITTLESS OF WPC

Wood used in WPC is most often in particulate form (e.g., wood flour) or very short fibers. Using wood flour as filler in these composites increases the composites' stiffness, and at the same time, reduces their toughness. Saline coupling agents were used to treat wood fibers, which were then blended with linear low density polyethylene (LLDPE) (Raj *et al* 1989). The Izod impact strength of the composites decreases sharply when the wood fiber content was higher than 20%wt (weight). It was also reported that the addition of wood flour (WF) with a particle size of 147μm can significantly increase the brittleness of LLDPE/WF composites (Marcovich and Villar 2003). Raj and Kokta (1992) also reported that the Izod impact strength of HDPE/wood fiber composites decreases with wood fiber content. The elongation-at-break and Charpy unnotched impact strength of LDPE/WF composites are very low though they can be improved with adding MA-g-styrene ethylene butylene triblock copolymer (MA-g-SEBS) as a compatibilizer (Oksman and Lindberg 1998). Lai and coworkers investigated the effects of four coupling agents (MA-g-LLDPE, MA-g-HDPE, MA-g-SEBS and MA-g-PP) on the mechanical properties of HDPE/WF composites (Lai *et al.* 2003). However, the notched Izod impact strength of the composites was lower than 90J/m although it was improved with the addition of coupling agent except for MA-g-PP. Dalvag and coworkers showed that the PP/WF composites were brittle though their impact strengths could be improved by a compatibilizer MA-g-PP (Dalvag *et al*.1985). However, another

study was reported that the impact strength of the composites PP-WF was decreased with addition of a MA-g-PP (Myers et al 1991). The effect of particle size on properties of PP-WF composites with 40wt% WF was investigated in the size range from 50 to 500μm (Start and Berger 1997). The notched Izod impact strength is basically independent of particle size. The composites with notched Izod impact strengths in the range from 15 to 22J/m are very brittle. The aspect ratio of the wood particles also had little effect on impact strength (Stark and Rowlands 2003). The notched Izod impact strength of recycled PP/WF composites increased slightly with WF content (Li *et al*. 2001). However, the composites with notched Izod impact strengths ranging from 19 to 23J/m are still very brittle. Dalväg and colleagues tried five types of elastomers, ethylene vinyl acetate copolymer (EVA), chlorinated PE (CPE), ethylene propylene copolymer (EP), etc., to toughen PP/WF composites (Dalväg *et al* 1985). Only a limited effect on improvement of impact strength of WPC was found. Oksman and Clemons employed rubbers, ethylene-propylene-diene terpolymer (EPDM) and MA-g-EPDM or MA-g-SEBS, to toughen PP/WF composites, where the ratio of PP to rubber was about 5/1 by weight (Oksman and Clemons 1998). The notched Izod impact strength increased from 20 to 55J/m with rubber content. The toughness of the toughened composites was still much lower than 100J/m. Dingova and coworkers studied the possibility of improving the properties of PP/WF composites by using EPDM both as a compatibilizer and coupling agent in quantities of 10, 20 and 30% (relative to PP mass). The Izod impact resistance values were increased for all test composites, but most of all were in the case of composite with 30% of EPDM (Dingova *et al.* 1998).

Creation of stress concentrations at fiber ends and poor interfacial adhesion

between wood and synthetic polymer have been recognized as the leading causes for embrittlement of the polymer matrix when the filler (wood flour) is added. Techniques for improving toughness of the composites include increasing the matrix toughness, optimizing the interface between the filler and the matrix through the use of coupling agents, introducing impact modifiers, and optimizing the filler-related properties. Although considerable work on optimizing the interface has been performed, much less work has been done on developing a consistent analysis for WPC using advance methods (for example FEM), especially experimental test methods. Until now no standard test methods for evaluating fracture behavior of WPC have been developed.

1.3 OBJECTIVES

The purpose of this thesis was to provide a numerical model for fracture behavior of wood plastic composite, based on statistical technique and finite element method. In accomplishing this goal, the following specific objectives were met:

1) To analyze the effect of fiber orientation and stress concentration factor on impact strength of WPC;
2) To develop an experimental procedure to study fracture toughness of wood plastic composite;
3) To simulate the fracture behavior of wood plastic composite using a finite element model; and
4) To validate the model using converging check and patch test.

1.4 OUTLINE OF THESIS

This thesis contains four chapters. Chapter 1 is a general introduction to this thesis in which development of history of WPC, brittleness of WPC, and objectives are

presented. In chapter 2, the result of impact strength of WPC by applying the fracture mechanics concept and by using statistic technique is shown. In chapter 3, an experimental test method is described to characterize the fracture toughness of WPC and finite element method (FEM) is introduced to simulate a four point bending model to evaluate stress intensity factor. In chapter 4, the conclusions for the experimental tests and finite element analysis are shown. Finally SAS codes for impact test and ANSYS outputs for a four point bending simulation are presented at appendix.

1.5 REFERENCES

Brown, W. F., Jr., and J. E. Srawley. 1966. Plane strain crack toughness of high strength metallic materials, ASTM STP 410, American Society for Testing and Materials.

SSAD, N., C. Olagnon, R. Estevez, and J. Chevalier. 2003. Experimental analysis of glassy polymers fracture using a double notch four point bending method. F. Polym. Composites and Adhesives II 22-38.

Keener, T. J., R. K. Stuart, and T. K. Brown. 2004, Maleated coupling agents for natural fibre composites. Composites: Part A 35 357-362

Oksman, K., H. Lindberg and A. Holmgren. 1998. The nature and location of SEBS-MA compatibilizer in polyethylene-wood flour composites. J. Appl. Polym. Sci. 69: 201-209

Dalvag, H. C. Klason and H. –E. Stromvall. 1985. The efficiency of cellulosic fillers in common thermoplastics. Part II Filling with processing acids and coupling agents. I. J. Polym. Mat. 11:9-38

Jang, B. Z. and Uhlmann D. R., and Vander Sande. J. B. 1985. Rubber-toughening of polypropylene. J. Appl. Polym. Sci. 25:2485-2504

Eckert, C. 2000. Opportunities for natural fibers in plastic composites. In:Proc. Progress in woodfibre-Plastic Composite, Toronto, ON.

Gupta, A. K., Ratnam B. K., and Srinivasan K. R. 1992. Impact toughening of polypropylene by ethylene vinyl acetate copolymer, J Appl Polym Sci, 45:1303-1312

Raj, R. G., B. V. Kokta, and B. Sanschagrain. 1989. Compounding of cellulose fibers with polyethylene: Effect of fibers treatment on dispersion in the polymer matrix. J. Appl. Polym. Sci. 38:1987-1996

Raj, R.G., B. V. Kokta, and C. Daneault. 1989. Effect of chemical treatment of fibers on the mechanical properties of polyethylene-wood fiber composites. J. Adhesion Sci. and Tech. 3(1):55-64

Raj R.G, and B. V. Kokta 1992. Thermomechanical properties of polyethylene-wood fiber composites, ACS Symposium Series 489:99-117

Myers, G. E., I. S. Chahyadi, C. Gonzalez, C. A. Coberly and D. S. Ermer. 1991. Wood flour/polyethylene or high density polyethylene composite: Influence of maleated polyethylene concentration and extrusion temperature on properties. I. J. Polym. Mat. 15:171-186

Kristiina oksman and Craig clemons 1998, Mechanical Properties and Morphology of Impact Modified Polypropylene-Wood Flour Composites, journal of Applied polymer science, Vol. 67, 1503-1513

Stark N. M. and Berger 1997 Investigations of species effects in an injection molding grade wood filled polypropylene. In: Proc. Woodfiber-Plastic Composite Conf. Forest Prod. Soc., Madison, Wis.

Dingova, E., Djiporovic, M., Miljkovic, J. 1998. Effect of EPDM modification on some properties of polypropylene wood flour composite, Material Science Forum, 303-308 pp.

Wolcott, M. P. and T. Adcock. 2001. New advances in wood fiber-polymer formulations. In: Proc. Wood-Plastic Conference. Plastics Technology Magazine and Polymer Process Communications. 107-204 pp.

Smith, P. M. 2001. U.S. woodfiber-plastic composite decking market. In: Proc. Sixth International Conference on Woodfiber-Plastic Composites. Forest Prod. Soc., Madison, WI. Pp. 13-17.

Tanguy, B. and Besson J. 2002. An extension of the Rousselier model to viscoplastic temperature dependent materials. I. J. F. 116: 81-101.

CHAPTER 2. IMPACT STRENGTH OF WOOD PLASTIC COMPOSITE (WPC)

2.1 INTRODUCTION

Toughness is an indication of the energy that a material can absorb before breaking and is usually measured by Izod and Charpy impact tests (Nielsen 1994). For a composite, the impact strength depends on the composition and structure as well as the testing method. For most composites, as the static strength increases, the toughness decreases. Thus, it might be implied that as the degree of adhesion increases, the toughness should be decreased. While this is generally true for continuous fiber reinforced brittle matrices, it is not always the case for short fiber reinforced ductile matrices, due to their complex fracture mechanisms (Kardos 1985). Impact fracture can be described as a process of crack initiation followed by crack propagation. A first order approximation of the total fracture energy can be determined by adding the different energy dissipating mechanisms (Clemons 1996). For notched samples:

$$W = W_f + W_m + \sum W_{mf} \qquad [2.1]$$

And for unnotched samples:

$$W = W_i + W_f + W_m + \sum W_{mf} \qquad [2.2]$$

where W_f and W_m are the work of fracture of fibers and matrix, respectively, Wmf terms are the work due to fiber/matrix interactions (sliding, debonding, fiber pullout, etc.), and W_i the crack initiation energy. A good interfacial adhesion enhances the resistance to crack initiation and decreases the stress concentration around the fiber ends and at the

poor adhesion area, thus tends to increase the impact strength. On the other hand, a good interfacial adhesion will facilitate the crack propagation along interfacial area and prevent the dissipation of energy and hence tend to decrease the impact strength. In addition, the fiber orientation relative to the impact load is also important for the interfacial adhesion to affect the impact strength. If the load is parallel to the fibers, the highest impact strengths are obtained if the adhesion is relatively poor and if the fibers are short. However, if the load is applied perpendicular to the fibers, good adhesion is required for even moderate impact strength. The antagonistic mechanisms of the interface and the complex behavior of the fibers make it difficult to obtain a consistent relationship between the interfacial adhesion and the impact strength for wood fiber/plastic composites (Myers 1991). Depending on the composition of composites and the types of impact tests, a good interphase can cause the apparent impact strength to either increase or decrease compared with a poor interphase, and one kind of impact test may generate a contradiction of the results of another type of test. Because of the complex mechanisms involved in the impact fracture, almost all of the correlations between the impact strength and the interfacial adhesion are specific to the systems under special conditions and can not be totally representative (Nielsen 1994).

Impact tests are employed to measure the ability of a specimen or a finished component to withstand a sudden blow. In many applications, a satisfactory resistance to impact loading is an important performance requirement and, indeed, impact toughness is often the deciding factor in materials selection. The traditional method of assessing whether a plastic is brittle or tough is to carry out an impact test, with a fast rate of loading to promote brittle failure. The test is quick and easy to carry out and can provide

data for comparing different materials under the conditions of test. The main test factors are the amount of energy available for breaking the specimen, the test temperature, stress concentrations and fiber orientation. There are many additional factors; details may be found in Brown (1981). The importance of impact testing is that such tests frequently indicate that many polymers which appear to exhibit tough, ductile failures when tested by tensile loading at a low or moderate strain-rate may suffer brittle fracture under impact loading when the strain-rate is relatively high. Brittle fracture, which is accompanied by relatively low energy absorption by the material, is obviously a mode of failure which design engineers generally wish to avoid. Over the years a large number of empirical impact tests have been devised to measure the impact strength of materials and components. However, the impact strength is not a fundamental material property apart from depending upon the specimen geometry as it also depends upon the particular test method employed. Thus, it is difficult to correlate the results obtained from different test techniques and extremely difficult to correlate the results from impact tests on specimens of the material to the impact performance of the manufactured article. This is the main reason why many investigators spend a great deal of time on conducting impact tests on the finished component. An interesting development, therefore, is the application of fracture mechanics theories to impact tests, notably by Brown (1973), Marshall *et al*.(1973), and Plati & Williams (1975), which has enabled two of the standard test methods to be directly correlated. The contributions of various components (fiber, polymer and interphase) may not be differentiated directly from the impact strength, but with the help of complementary techniques, considerable qualitative information on microstructure and fracture mechanisms can be obtained. Clemons (1999) reported that

the addition of MPP (maleated polypropylene) as a compatibilizer that improved the interfacial adhesion had different effects on the impact strength of composites containing wood fibers with different aspect ratios. For shorter fiber composites, the interfacial adhesion had no significant influence on the notched impact strength. While for long fiber composites, the substitution of fiber breakage (W_f) due to improved adhesion for fiber pullout (a component of $\sum W_{mf}$) results in an overall reduction in notched impact performance. On the other hand, the unnotched impact strength of the composites containing either fibers are significantly increased due to improved stress transfer allowing for efficient distribution of applied stress and inhibiting the formation of cracks. This trend, (i.e., an increase in interfacial adhesion or more exactly in static strength) is generally associated with a greater decrease in notched impact strength and a smaller decrease or even an increase in unnotched impact strength. In a first order approximation, it can be said that notched impact energy is a measure of crack propagation and unnotched impact energy is a measure of both crack initiation and propagation. There are two standard methods to measure impact strength of materials. One is the Charpy impact test. Charpy V-notch tests are used to measure the fracture toughness of materials. The notched bar is subjected to an impact with a striker moving at about 5m/s. In the ductile regime, inertial effects can be neglected (Tvergaard and Needleman, 1988; Sainte Catherine *et al*., 2001) but the variations of flow strength with temperature and strain rate play an important role on energy dissipation (Mathur *et al*., 1994). Charpy V-notch specimens were tested using an instrumented Charpy testing device at -60 ºC (Tanguy 2001). Specimens were machined and tested according to the AFNOR90 standard (AFNOR 1990). The other method is the Izod impact test. During the first part of 20th

century, a metallurgist named Izod invented an impact test for determining the suitability of various metals to be used as cutting tools. The test involved a pendulum with a known weight at the end of its arm swinging down and striking the specimen as it stood clamped in a vertical position. Notched Izod Impact is a single point test that measures a material resistance to impact from a swinging pendulum. Izod impact is defined as the kinetic energy needed to initiate fracture and continue the fracture until the specimen is broken. Izod specimens are notched to prevent deformation of the specimen upon impact. This test can be used as a quick and easy quality control check to determine if a material meets specific impact properties or to compare materials for general toughness.

The fracture behavior of composites is affected by many variables, including the nature of the fiber and matrix, the fiber-matrix bond, fiber distribution and orientation, etc. Some possible damage modes in composites are matrix cracking, interfacial bond failure, fiber breakage, void growth and delamination (Clemons 1996). Scanning electron microscopy (SEM) may be one of the best ways to reveal all of these failure modes owing to its superior depth of field. Based on the fracture modes, the strength of the interfacial adhesion relative to the individual components can be readily evaluated qualitatively, especially the role of compatibilizers or manufacturing procedures intended to improve the interfacial adhesion. In general, fiber pullout and clean surface of the fiber are associated with poor interfacial adhesion, while matrix cracking and fiber breakage imply that the interfacial bonding is greater than the strength of individual components. The treatment of cellulose fibers with silanes produced significant increases in interfacial adhesion leading to the breaking and delamination of cellulosic fiber when the PP composites are stretched. High magnification SEM is enable to show the existence of

characteristic bridging between the PP and the cellulosic fibers (Bataille, 1989). From the fractured surface of LDPE composites the untreated fibers appeared to be pull out of the matrix and free of any matrix material adhering them, a clear indication of poor fiber-matrix adhesion. When the fibers were treated with a silane, the failure mode was matrix shear yielding flow (Herrera 1997).

2.2 OBJECTIVES

With the increasing use of WPC in structural engineering applications it is becoming essential to have as complete an understanding as possible of the failure mechanisms. The study of fracture surfaces can lead to an understanding of the source of the fracture and the relation between the mode of crack propagation and micro structure of the material.

The purpose of this chapter was to investigate the effect of stress concentration factor and fiber orientation on impact strength of WPC, based on statistical technique and SEM. In accomplishing this goal, the following specific objectives were met:

1) To analyze the effect of fiber orientation and stress concentration factor on impact strength of WPC by statistic technique; and
2) To characterize the fracture modes to evaluate the fracture mechanism of WPC by SEM.

2.3 MATERIALS AND METHODS

2.3.1 Material Selection

To investigate impact strength of WPC, commercial wood plastic composite was used. The material sampling for this study consisted of sixty density specimens and fifty eight impact specimens. Density test specimens were sampled into two groups based on

fiber orientation. Impact specimens were also divided into two groups by the same criterion. Every specimen was conditioned at 23±2°C and 50±5% relative humidity in a conditioning chamber for five days before testing.

2.3.2 Density Testing

Density properties of WPC were measured according to the ASTM D638 (ASTM 2000). For density tests, two different fiber orientation specimens were prepared. Namely, density of one group was measured along the machine direction (parallel fiber orientation), while that of the other group was measured along the cross machine direction (perpendicular fiber orientation). To obtain the mean value of density of each group, a total of sixty specimens were used. The dimension of density specimens was prepared to be 64mm by 13.5mm by 4.5mm. QMS Density profile system was used to get 2D density profile of WPC. Density determination by scanning densitometers is based on the relationship of x-ray attenuation and density, as expressed in the following equation:

$$\frac{I}{I_0} = e^{-\mu_m \cdot \rho \cdot t} \qquad [2.3]$$

where: I = intensity of radiation beam after passing through the sample (counts)
I_0 = intensity of radiation beam without passing through the sample (counts)
μ_m = material mass attenuation coefficient (m^2/kg)
ρ = material density (kg/m^3)
t = material thickness (mm)
e = natural logarithm base

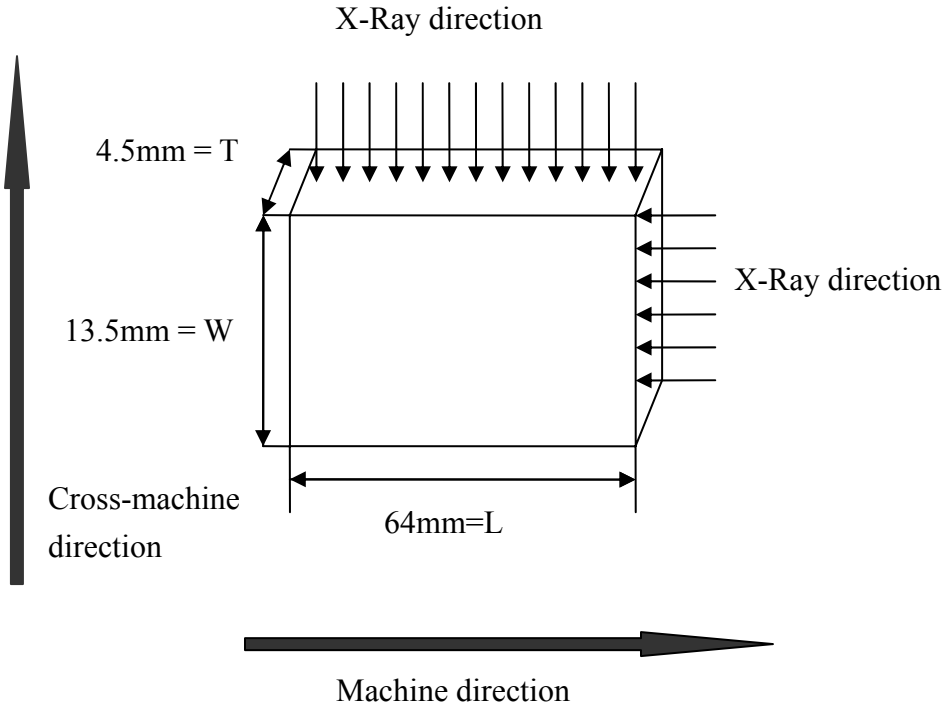

Figure 2.1 Schematic of two dimensional density measurements by x-ray scanning technique showing the machine direction (fiber orientation parallel to the machine direction) and cross machine direction (fiber orientation perpendicular to the cross machine direction)

2.3.3 Impact Testing

For the impact tests, a pendulum impact test machine (Model 892 from Tinius Olsen Company) was employed, which is smaller versions of that used for metals, and supplies a fixed amount energy (fixed mass and length of pendulum) at a fixed speed. According to the ASTM standard D 256, 58 impact specimens were cut to a nominal size of 64×12.7×4.2mm. The samples were divided into two groups by the fiber orientation.

In both groups, five different notch depths of the specimen were prepared to be 1, 2, 3, 4, and 5 mm. Tests were made over the service temperature range (20°c ±5) on unnotched and notched bars. Notched bars had a 45° notch with fixed notch-tip radius (0.25mm). The specimen was clamped into pendulum impact test fixture with the notched side facing the striking edge of the pendulum. The pendulum was released and allowed to strike through the specimen. Izod specimens were tested as cantilever beams. The ASTM impact energy is expressed in J/m or ft-lb/in. Impact strength is calculated by dividing impact energy in Joule by the thickness of the specimen. The test result was typically the average of the five specimens. The linear elastic stress concentration factor k is given by

$$k = 1+2\sqrt{(a/r)} \qquad [2.4]$$

where : a = length of notch (mm)
r = radius of the notch tip (mm)
k = stress concentration factor (scf)

Two-way ANOVA was used to investigate the effect of stress concentration factor and fiber orientation to the load head on impact strength of WPC. Proc mixed command was used to determine degree of freedom of total variables for an unbalanced design using statistic analysis software (SAS). To check difference of each variable effect on impact strength of WPC, Tukey adjustment test was carried out. Null hypothesis was that stress concentration factor, fiber orientations, and combining two did not affect impact strength of WPC. A p-value of less than 0.05 was deemed to be statistically significant for the effects.

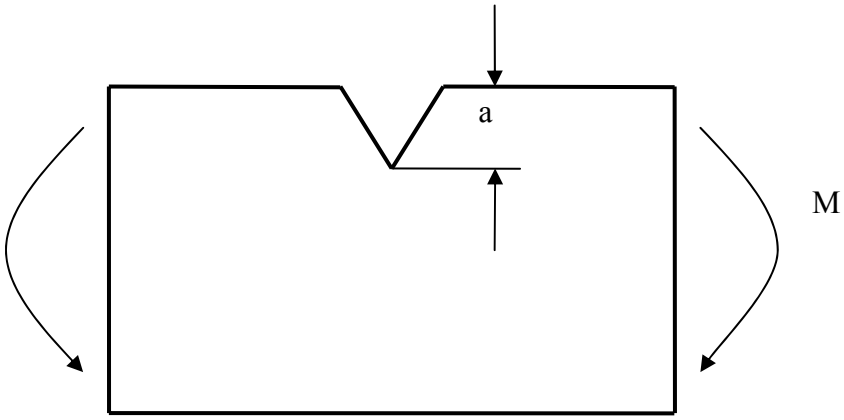

Figure 2.2 A model of stress concentration factor for WPC with a as notch depth and M as bending moment

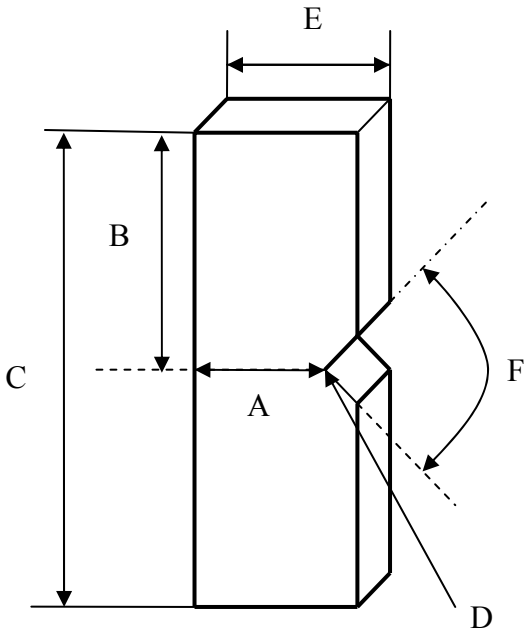

A: 10.2±0.05mm
B: 32±1mm
C: 64±2mm
D: 0.25R±0.05
E: 12.7±2mm
F: 22.5±0.5º

Figure 2.3. Schematic of impact specimens based on ASTM Standard D 256. The same sample dimensions for tests perpendicular and parallel to the major fiber orientation direction.

2.3.4 Fracture Surface Analysis of WPC by Scanning Electron Microscopy

The fracture surface of impact specimens was examined by a Hitachi S2500 scanning electron microscope (SEM) operating at 15kV. The samples were cut to have 5 mm thickness and spotted with gold. The SEM micrographs were then used for the investigation of the effect of fiber orientation on impact strength of WPC. The analysis was carried out using a computerized image analyzer

2.4 RESULTS AND DISCUSSION

2.4.1 Density Test Result

As expected, wood plastic composite manufactured by extrusion method had highly uniform density distribution within one direction. However, there was some difference in density between two directions which affect mechanical properties of wood plastic composites. Compared to that of the machine direction of WPC, the mean density value of cross machine direction of WPC was 6% higher (Figure 2.4). More specifically saying, the mean mass attenuation (μ_m) in the cross machine direction was higher than the mean mass attenuation (μ_m) along the machine direction. It was assumed that more wood fiber content by unit volume was in cross machine direction due to the processing parameter. Also, it is interesting to note that the nucleation density on the wood fiber surface was remarkably higher than in the bulk phase, and a transcrystalline layer could be developed around the fiber (Wolcott 2000). In general, transcrystalline zones are formed parallel to the flow direction where the fibers are predominantly oriented during processing (Hata 1993). Increased transcrystallinity may thus explain the higher storage modulus of WPC. This would lead to a higher modulus in the direction of flow (same as the testing direction) because of the higher stiffness of the transcrystalline morphology (Moginger 1991).

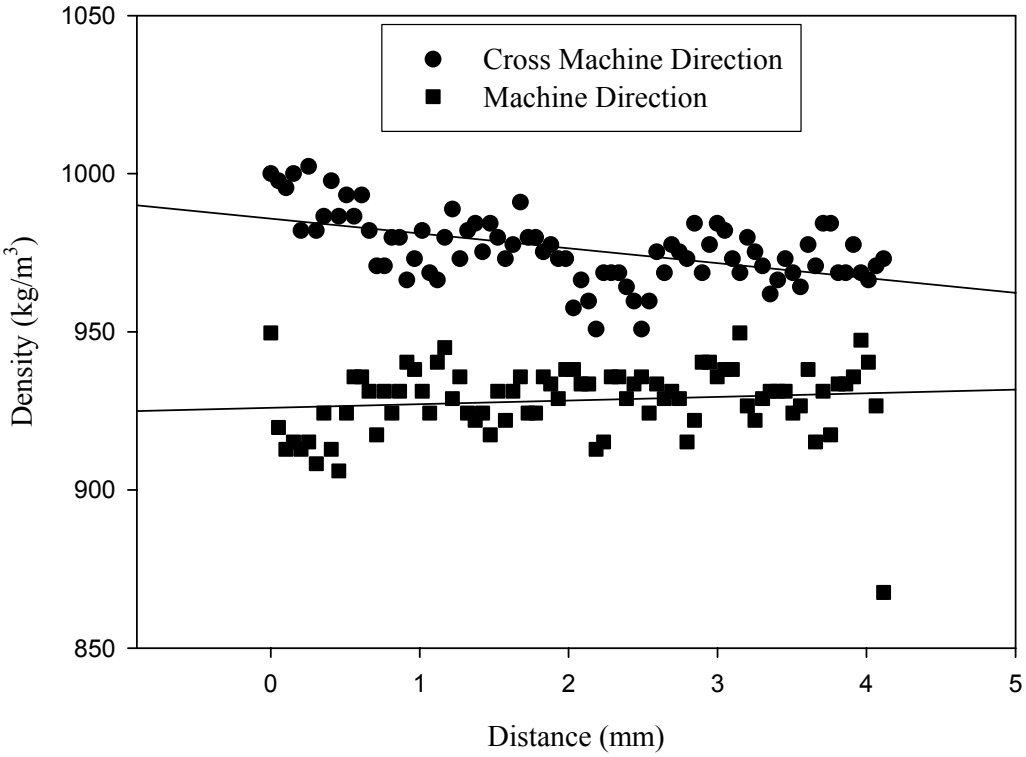

Figure 2.4 Density variation between two fiber orientations (machine direction and cross machine direction)

2.4.2 Impact Strength

Six different notch lengths were converted to stress concentration factor using Equation (2.2) (Table 2.1 and Table 2.2). Stress concentration factor had a linear relationship with impact strength and break energy of WPC. As stress concentration factor increased, impact strength and break energy of WPC decreased (Figure 2.5). Two different fiber orientations to the load head also had significant effect on the impact strength of WPC. Impact strength and break energy of the WPC of the fiber perpendicular to the load head showed 37% and 45% higher than its counterpart. This result corresponds with the fact that the crack propagates more easily along the

interfacial area of WPC (Stark and Berger 1997), and compared to the cross machine direction specimen, the machine direction specimen has more exposed area of interfacial area to impact loading. As impact wave met different phases such as fiber, polymer, and voids in the cross machine direction, it would lose its energy as dissipation energy. However, impact wave could go along interfacial area without much loss of impact energy along the machine direction. Statistical techniques were employed to analyze the effect of stress concentration factor, fiber orientation, and combining both on the impact strength of WPC. Two-way ANOVA (analysis of variance) test results were obtained from the SAS. A summary of ANOVA results for the effect of stress concentration factor and fiber orientation to the load head on the impact strength of wood plastic composite are shown in Table 2.3. According to Table 2.3., correlation of the combing effect is 93% and each of the variables has a significant effect on the impact strength of WPC. The p-value for stress concentration factor, fiber orientation to the load head, and combing effect was <.0001. Therefore, the null hypothesis was rejected. Difference in impact strength of wood plastic composite as a result of stress concentration factor and fiber orientation to the load head were determined using Tukey's test. The results of Tukey's test are summarized in Table 2.4. According to the p-value in Table 2.4, each parameter had a significant effect on impact strength of WPC except the comparison 8.26 with 9 in stress concentration factor. The p-value was 0.9742 in Tukey's test. Degree of freedom in the test was 46 which were adjusted by Proc mixed command in SAS for an unbalanced design. Standard deviation (S.T.D) in each comparison of the stress concentration factor on impact strength was about 2. Standard deviation (S.T.D) in comparison of the fiber orientation effect on impact strength was less than 2.

Table 2.1 The effect of parallel fiber orientation to the load head and stress concentration factor on impact strength of WPC

Parallel fiber direction to the load head									
I.D.	a (mm)	t (mm)	w (mm)	d (mm)	r (mm)	S.C.F	Density (kg/m^3)	B.E. (J)	I.S. (J/m)
1	0	4.13	13.58	13.58	0.25	1	920.8	0.12	43.0
2	1	4.13	13.57	12.57	0.25	5	939.6	0.13	33.7
3	2	4.18	13.65	11.65	0.25	6.66	922.8	0.12	30.7
4	3	4.28	13.57	10.34	0.25	8.18	918.2	0.10	25.2
5	4	4.40	13.66	9.66	0.25	9	937.3	0.11	25.7
6	5	4.48	13.78	8.78	0.25	9.94	928.7	0.09	20.8

Table 2.2 The effect of perpendicular fiber orientation to the load head and stress concentration factor on impact strength of WPC

Perpendicular direction to the load head									
I.D.	a (mm)	t (mm)	w (mm)	d (mm)	r (mm)	S.C.F	Density (kg/m^3)	B.E. (J)	I.S. (J/m)
1	0	4.49	13.57	13.57	0.25	1	974.6	0.36	81.7
2	1	4.41	13.41	12.41	0.25	5	982.2	0.22	51.7
3	2	4.39	13.55	11.55	0.25	6.66	980.5	0.19	45.1
4	3	4.49	13.57	10.43	0.25	8.18	979.3	0.16	36.6
5	4	4.44	13.62	9.62	0.25	9	986.1	0.16	36.2
6	5	4.46	13.64	8.64	0.25	9.94	979.3	0.14	31.9

* S.C.F - stress concentration factor
* B.E. - break energy
* I .S. - impact strength

Table 2.3 Summary of a two-way ANOVA (analysis of variance) for impact strength of WPC

Source	DF	Sum of Square	Mean Square	F	Pr>F
Model	11	14363.771	1305.797	64.31	<.0001
Error	46	2373.501	20.304		
Corrected Total	57	15297.759			

R-Square	Coeff Var	Root MSE	Mean(IS)
0.938	11.614	4.506	38.795

Source	DF	Type I SS	Mean Square	F	Pr>F
scf	5	8477.106	1695.421	83.50	<.0001
dir	1	4447.152	4447.152	219.03	<.0001
scf*dir	5	1439.513		14.18	<.0001

Source	DF	Type III SS	Mean Square	F	Pr>F
scf	5	8105.392	1621.078	79.84	<.0001
dir	1	4261.021	4261.021	209.86	<.0001
scf*dir	5	1439.513	287.902	14.18	<.0001

* DF – degree of freedom
* scf – stress concentration factor
* dir – fiber orientation to the load head
* F – F statistic taken as 0.05 for rejection
* MSE – mean square error
* Type I SS – type I sum of square
* Type III SS – type III sum of square
* IS – impact strength

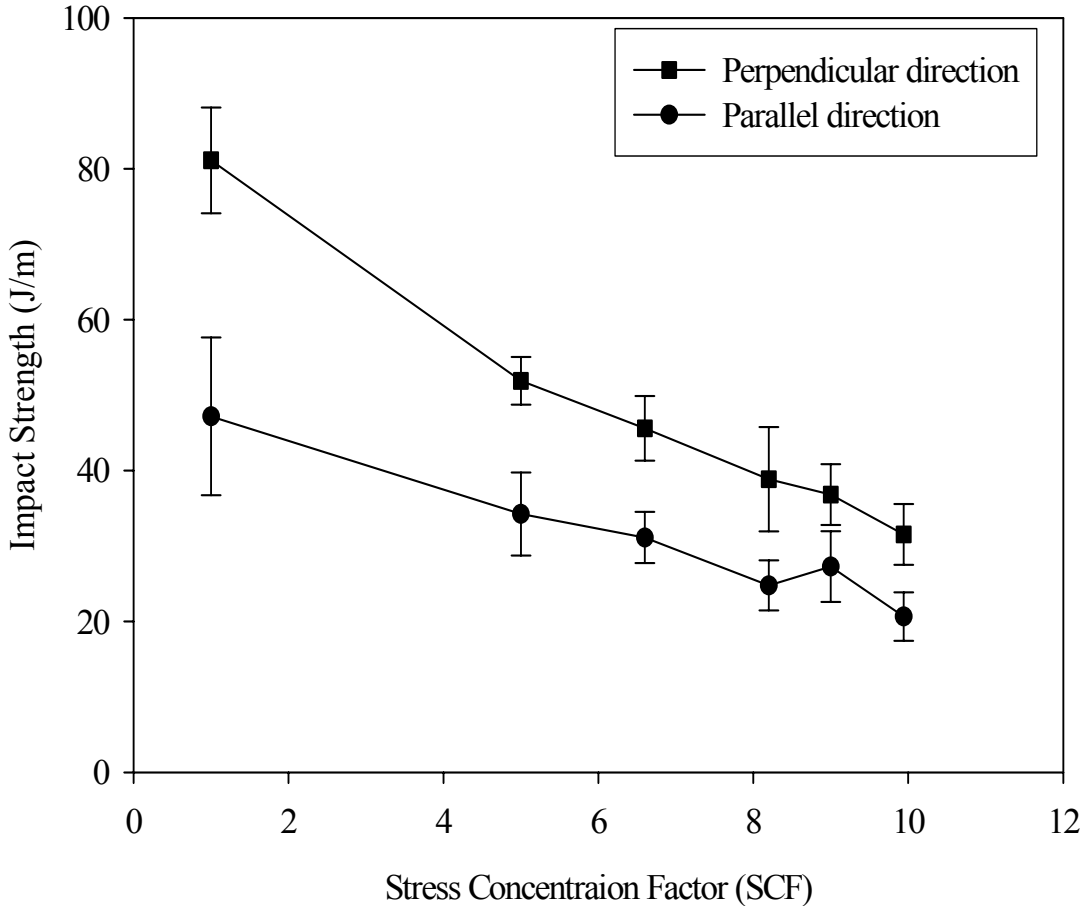

Figure 2.5 Impact strength of WPC as influenced by fiber direction and stress concentration factor (S.C.F)

Table 2.4 The results of difference of impact strength of WPC based on the effect of stress concentration factor and fiber orientation (Tukey's test)

Effect	scf	dir	_scf	_dir	Estimate	S.T.D	DF	t Value	Pr>|t|	Adjustment
scf	1		6.66		24.4516	2.0151	46	12.13	<.0001	Tukey
scf	1		8.26		31.4533	2.0151	46	15.61	<.0001	Tukey
scf	1		9		31.3878	2.0151	46	15.58	<.0001	Tukey
scf	1		9.94		36.0130	2.1766	46	16.55	<.0001	Tukey
scf	5		6.66		4.7874	2.0151	46	2.38	0.0217	Tukey
scf	5		8.26		11.7891	2.1766	46	5.85	<.0001	Tukey
scf	5		9		11.7236	2.0151	46	5.82	<.0001	Tukey
scf	5		9.94		16.3488	2.0151	46	7.51	<.0001	Tukey
scf	6.66		8.26		7.0017	2.1766	46	3.47	0.0011	Tukey
scf	6.66		9		6.9362	2.0151	46	3.44	0.0012	Tukey
scf	6.66		9.94		11.5614	2.1766	46	5.31	<.0001	Tukey
scf	8.26		9		-0.0655	2.0151	46	-0.03	0.9742	Tukey
scf	8.26		9.94		4.5597	2.1766	46	2.09	0.0417	Tukey
scf	9		9.94		4.6252	2.1766	46	2.12	0.0390	Tukey
dir		1		2	-17.316	1.1953	46	-14.4	<.0001	Tukey

* scf – stress concentration factor

* dir – fiber orientation (1 – Machine direction and 2 – Cross machine direction)

* _scf – stress concentration factor comparing with the stress concentration factor in the same row.

* _dir – fiber orientation comparing with the fiber orientation in the same row.

* Estimate – difference of the comparison

* S.T.D – standard error of the comparison

* DF – degree of freedom

2.4.3 Scanning Electron Microscopy Examination on Fracture Surface

The fracture surfaces of the specimens broken by impact loading were subjected to scanning electron microscopy (SEM) to determine the fracture path and the fracture modes in relation to its microstructure. Such information is valuable in identifying the fracture mechanism for analyzing the effect of fiber orientation to the load direction. In general, there were two ways in which WPC might fracture. If WPC was stressed parallel to the load head, fracture would occur with cracks running the interfacial area and pulling out the fiber from the matrix. Alternatively if the WPC was stressed in the direction perpendicular to the load head, the intermolecular cleavage occurs with the cracks running across fiber, interfacial area, and polymer and breaking the fibers. Compared to the fracture surface along the cross machine direction, the fracture surface along the machine direction had fairly tight matrix against the wood particles and were relatively free of voids (Figure 2.8). According to Figure 2.9, some wood fibers were pulled away from the matrix and a few had fractured in the machine direction. Therefore, when machine direction specimens was hit by the load head, less dissipation energy occurred which eventually resulted in lower impact strength. Cross machine direction specimens had more number of voids and had rough surface (Figure 2.11). When load head hit the cross machine direction specimens, the impact wave had to meet different phases more often such as fiber, interfacial area, polymer and voids. Dissipation energy occurred more often along the cross machine direction. From Figure 2.13, micro voids between fiber and matrix were assumed to consume the impact energy. The main fracture mechanism along the machine direction was fiber pullout and interfacial bond failure while the main fracture mechanism in the cross machine direction was fiber breakage.

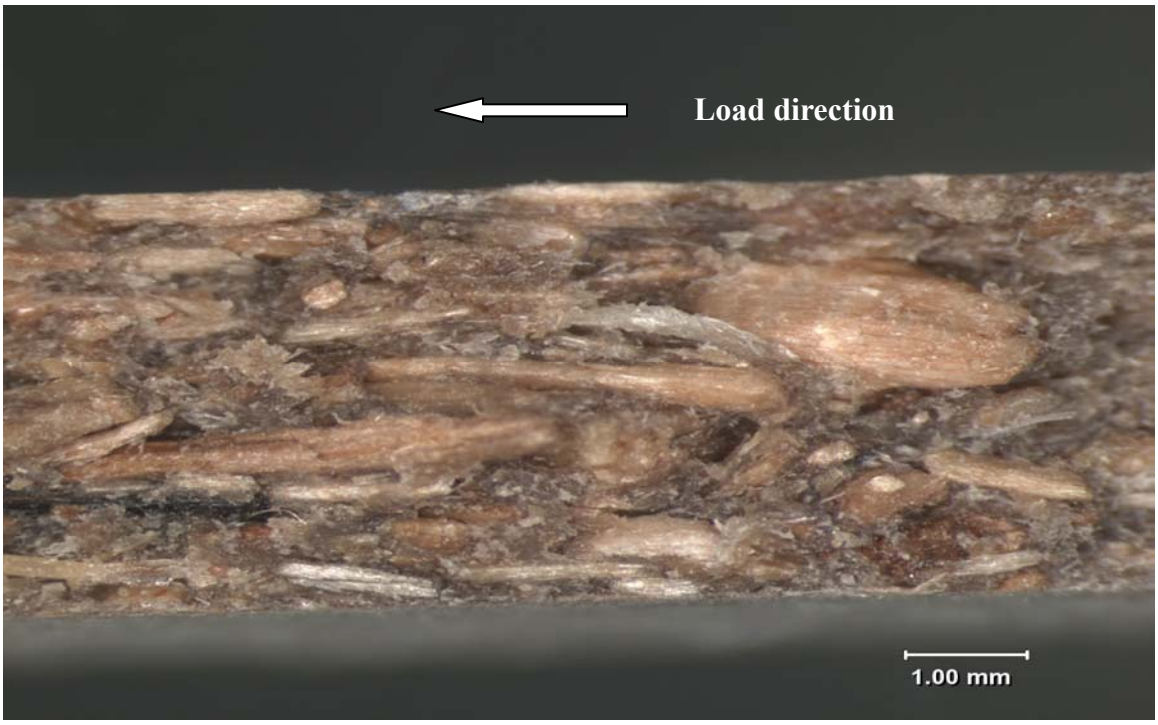

Figure 2.6 Impact fracture surface along the machine direction by an image analyzer (fiber orientation parallel to the load direction).

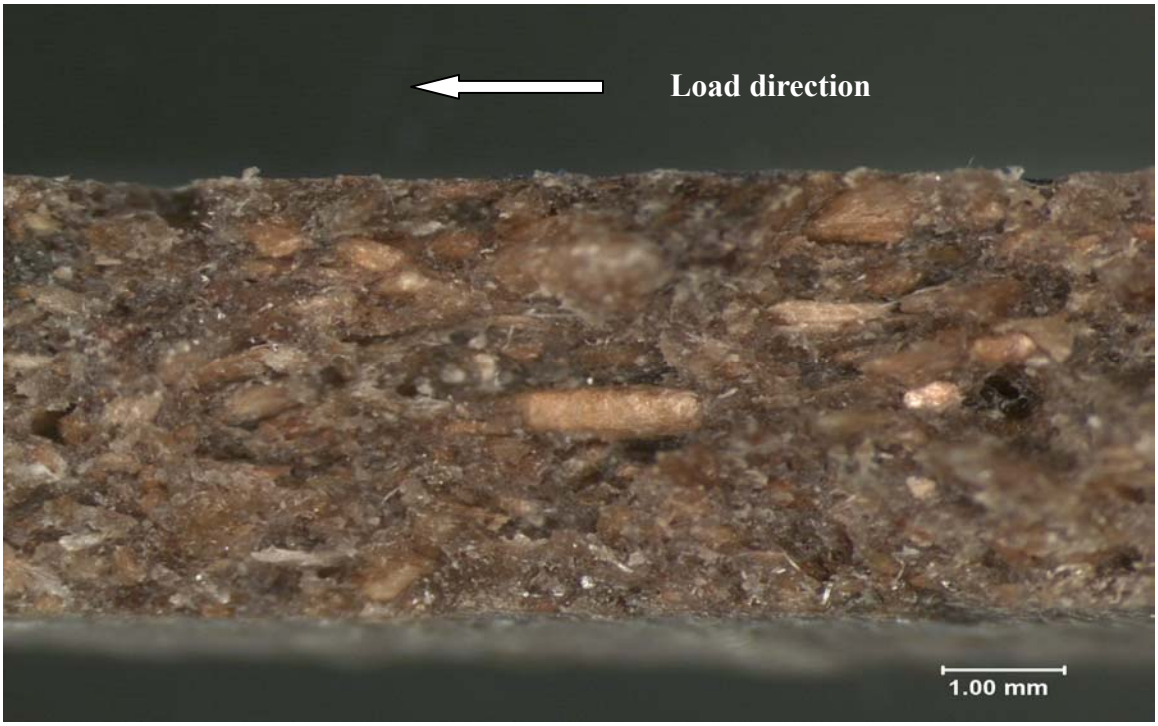

Figure 2.7 Impact fracture surface along the cross machine direction by an image analyzer (fiber orientation perpendicular to the load direction).

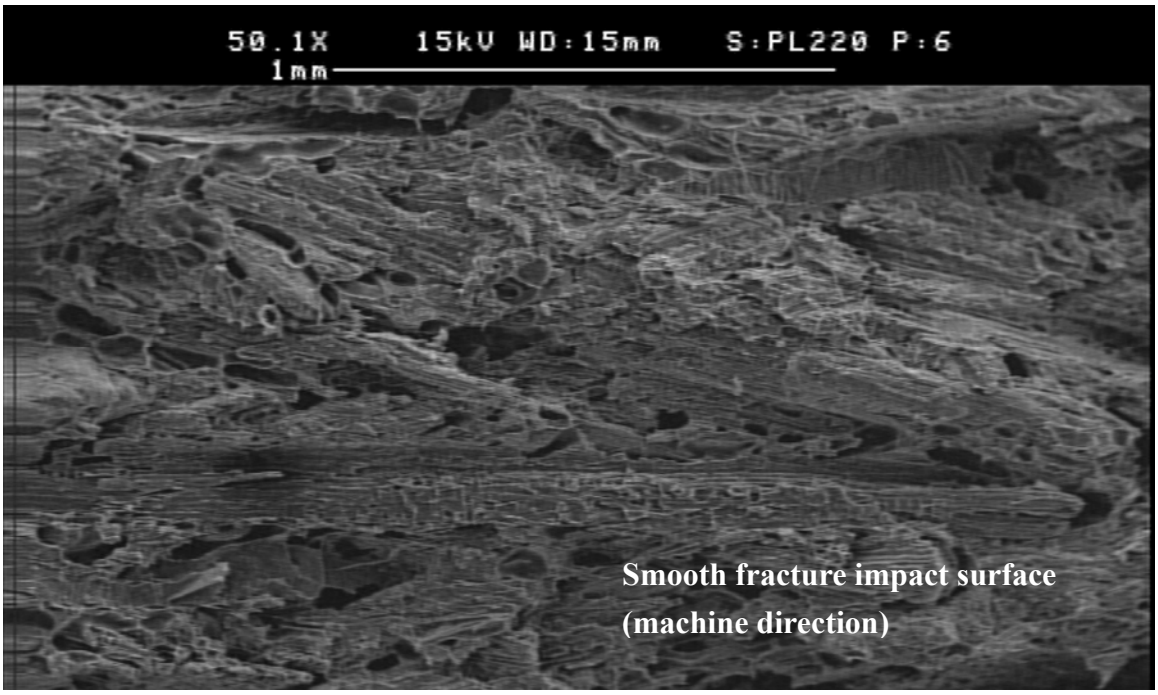

Figure 2.8 Fracture surface of impact specimen along the machine direction by SEM with magnification of 50x.

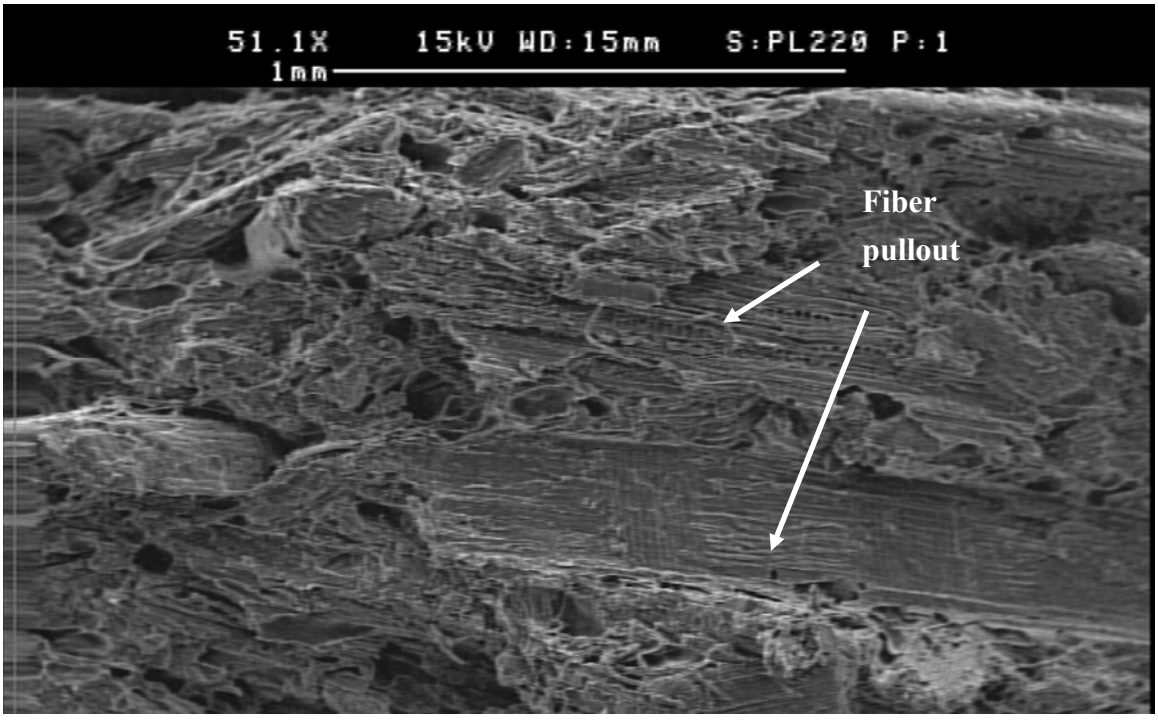

Figure 2.9 Fracture surface of impact specimen along the machine direction by SEM with magnification of 51x.

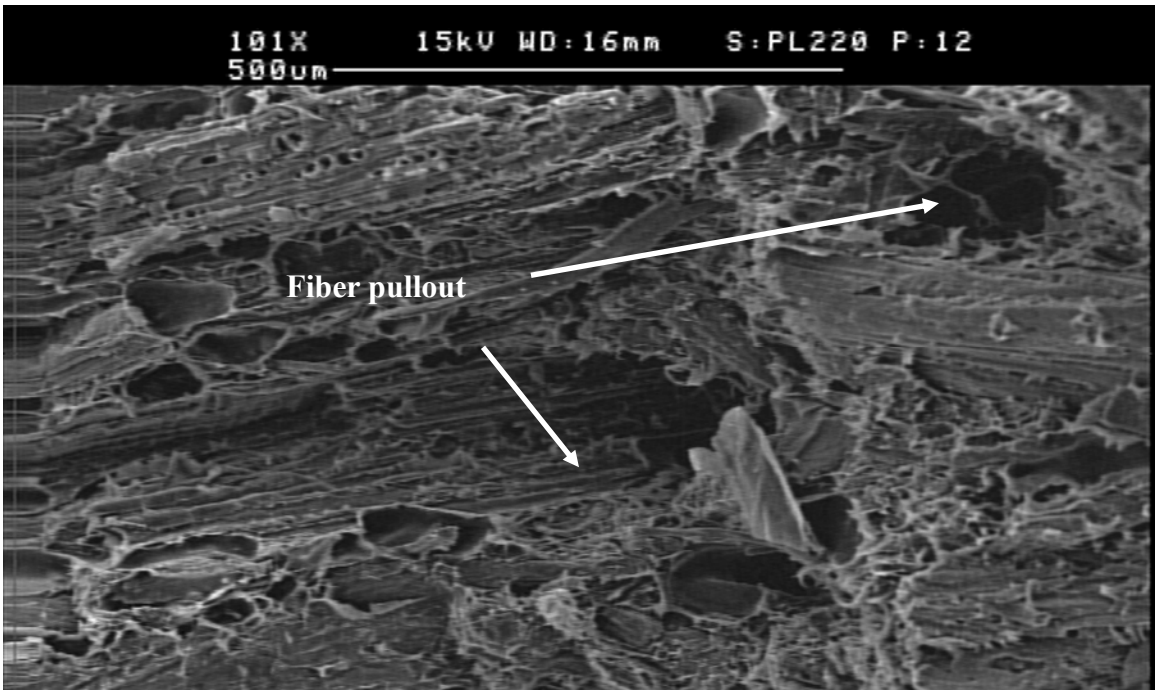

Figure 2.10 Fracture surface of impact specimen along the machine direction by SEM with magnification of 101x.

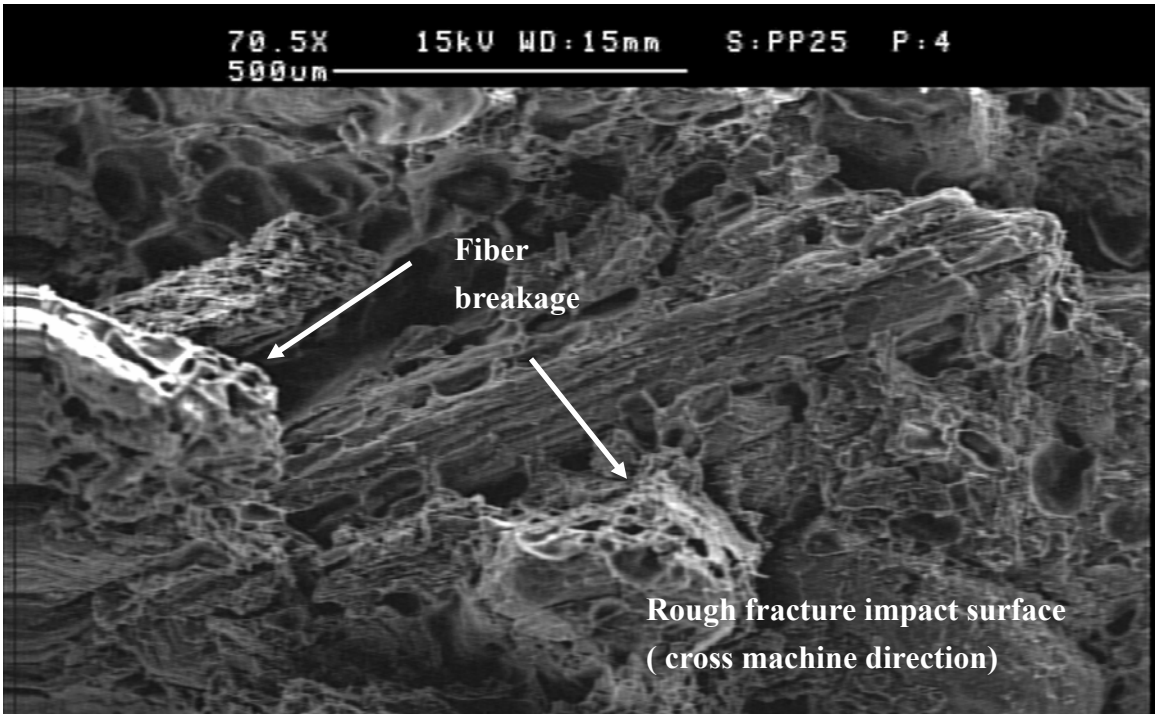

Figure 2.11 Fracture surface of impact specimen along the cross machine direction by SEM with magnification of 70x.

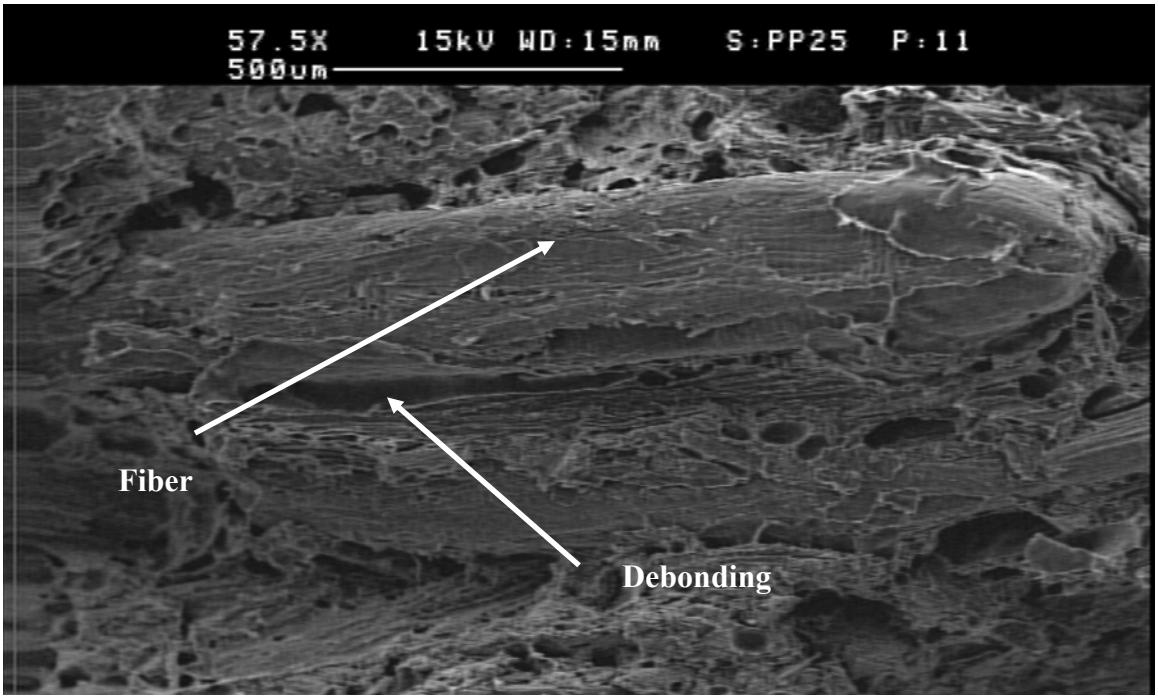

Figure 2.12 Fracture surface of impact specimen along the cross machine direction by SEM with magnification of 57x.

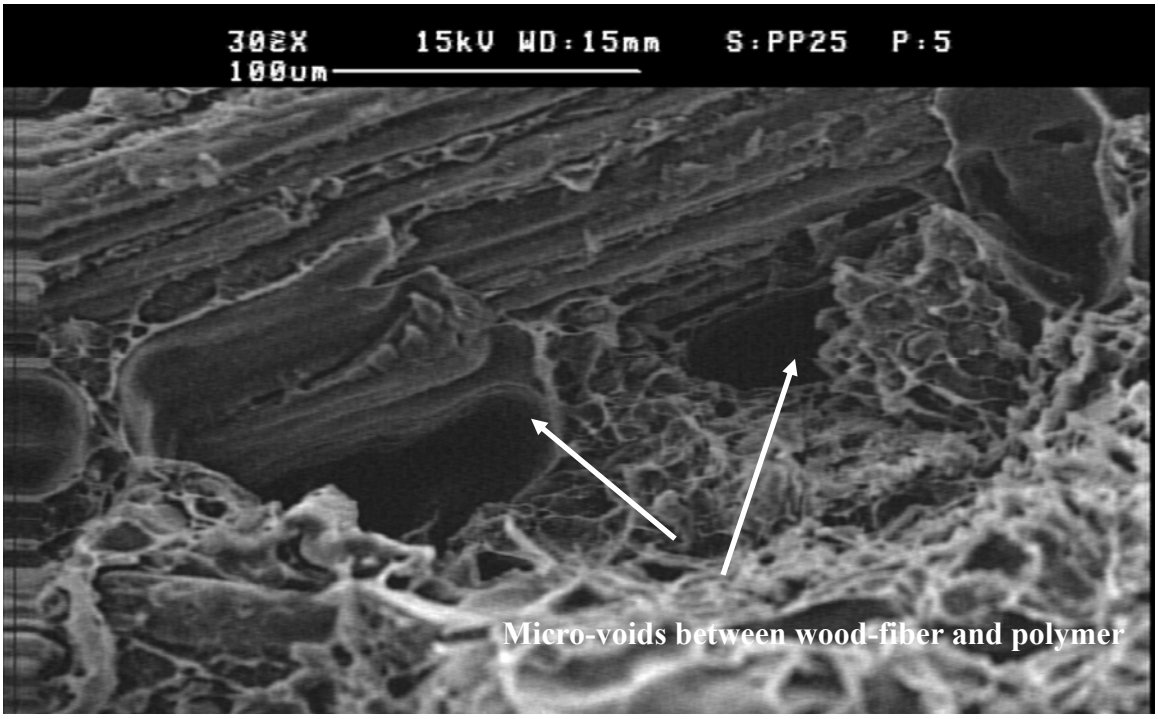

Figure 2.13 Fracture surface of impact specimen along the cross machine direction by SEM with magnification of 302x.

2.5 CONCLUSIONS

To analyze the fracture behavior of WPC, both experimental test and numerical method were employed. The density test results indicate that WPC made by the extrusion method had density variation in fiber orientation. The mean mass attenuation coefficient of WPC in the machine direction was 6% lower than that of WPC in the cross machine direction. The results of the impact test showed that compared to machine direction of WPC having the lower density value, cross machine direction having higher density value had better performance in those mechanical tests. Also as shown by the analysis of variance (ANOVA) and Tukey's test, the effect of stress concentration factor (S.C.F) and fiber orientation and combing effect on impact strength of WPC was significant. From the experimental test, it can be realized that fiber orientation is a key parameter on mechanical properties of WPC. Fracture surface examined by SEM showed that fracture surface along the machine direction had fewer voids and smooth surface compared to the surface along the cross machine direction. Fiber pullout due to impact energy occurred more frequently in impact specimens of the machine direction while fiber breakage happened more frequently in impacts specimen of the cross machine direction. Therefore, the material used in this study had weak bondage between polymer and fibers.

2.6 REFERENCES

SSAD N., C. Olagnon R. Estevez, and J. Chevalier. 2003. Experimental analysis of glassy polymers fracture using a double notch four point bending method, Fracture of Polymers, Composites and Adhesives II 22-38.

Keener T. J., R. K. Stuart, and T. K. Brown. 2004. Maleated coupling agents for natural fibre composites, Composites: Part A 35 357-362

Oksman, K. H., Lindberg, and A. Holmgren. 1998. The nature and location of SEBS-MA compatibilizer in polyethylene-wood flour composites. J. Appl. Polym. Sci. 69: 201-209

Dalvag H. C. Klason and H. E. Stromvall. 1985. The efficiency of cellulosic fillers in common thermoplastics. Part II Filling with processing acids and coupling agents. I. J. Polym. Mat. 11:9-38

Eckert C. 2000. Opportunities for natural fibers in plastic composites. In:Proc. Progress in woodfibre-Plastic Composite, Toronto, ON.

Gupta AK, Ratnam B.K., and Srinivasan K.R. 1992. Impact toughening of polypropylene by ethylene vinyl acetate copolymer, J. Appl. Polym. Sci. 45:1303-1312

Raj, R.G., B. V. Kokta and B. Sanschagrain. 1989. Compounding of cellulose fibers with polyethylene: Effect of fibers treatment on dispersion in the polymer matrix. J. of Appl. Polym. Sci. 38: 1987-1996

Raj, R.G., B. V. Kokta, and C. Daneault. 1989. Effect of chemical treatment of fibers on the mechanical properties of polyethylene-wood fiber composites. J. Adhesion Sci and Tech. 3(1):55-64

Raj R.G, and B.V. Kokta 1992. Thermomechanical properties of polyethylene-wood fiber composites, ACS Symposium Series 489:99-117

Myers, G. E., I. S. Chahyadi, C. Gonzalez, C. A. Coberly and D. S. Ermer. 1991. Wood flour/polyethylene or high density polyethylene composite: Influence of maleated polyethylene concentration and extrusion temperature on properties. I. J. Polym. Mat. 15:171-186

TANGUY B. and J. BESSON 2002. An extension of the Rousselier model to viscoplastic temperature dependent materials. I. J. F. 116: 81-101.

Oksman, K. and C. Clemons. 1998. Mechanical Properties and Morphology of Impact Modified Polypropylene-Wood Flour Composites, J. Appl. Polym. Sci. 67:1503-1513

Dubnikova I. L., S. M. Berezina, V. G. Oshmyan, and V. N. Kuleznev. 2003. Effect of interfacial adhesion on the deformation behavior and toughness of particulate-filled polypropylene. Polym. Sci. 45(9):1494-1507

Stark N. M. and Berger. 1997 Investigations of species effects in an injection molding grade wood filled polypropylene. In: Proc. Woodfiber-Plastic Composite Conf. Forest Prod. Soc., Madison, Wis.

Nielsen, L. E. and R. T. Landel. 1994. Mechanical properties of polymer and composites. Marcel Dekker, Inc. 307.

Bataille, P., L. Richard and S. Sapieha. 1989. Effects of cellulose fibers in polypropylene composites. Polym. Composites. 10(2):103-108

Dingova, E., M. Djiporovic., and J. Miljkovic. 1998. Effect of EPDM modification on some properties of polypropylene wood flour composite, Material Science Forum, 282-2:303-308

Wolcott M. P. and T. Adcock. 2000. New advances in wood fiber-polymer formulations. In: Proc. Wood-Plastic Conference. Plastics Technology Magazine and Polymer Process Communications. 107-204 pp.

Clemons, C. 1996. Exploratory microscopic investigation of impacted paper fiber-reinforced polypropylene composites. In WoodFiber-Plastic Composites: Virgin and Recycled Wood Fiber and Polymers for Composites. Eds. Caulfield, D. F., R. M. Rowell and J. A. Youngquist. pp 173-179.

Herrera, F. and M. D. Aguilar. 1997. Effect of fiber treatment on the mechanical properties of LDPE-henequen cellulosic fiber composites. J. Appl. Polym. Sci. 65(1):197-207.

CHAPTER 3. FRACTURE TOUGHNESS OF WOOD PLASTIC COMPOSITE (WPC)

3.1 INTRODUCTION

Basics to fracture mechanics is the understanding of the state of stress near the tip of a sharp crack and the relationship between gross stress and flaw geometry. The stress fields near crack tips can be divided into three basic types, each associated with a local mode of deformation, as shown in Figure 2.1. The opening mode, I, is associated with a local displacement in which the crack surfaces move directly apart. The shearing mode, II, is characterized by displacements in which the crack surfaces slide over one another. In mode III, tearing, the crack surfaces slide with respect to one another parallel to the leading edge. Mode I is the most critical mode and is the only one to be discussed in this study.

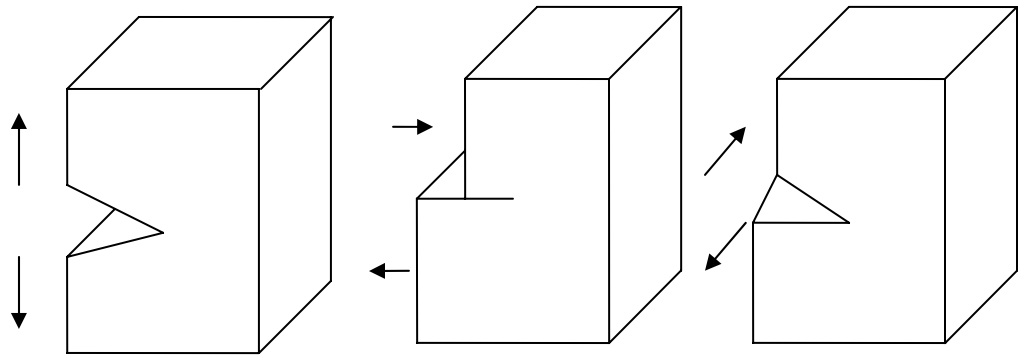

Figure 3.1 Modes of fracture for engineering materials under various loading conditions. (a) opening mode, (b) shearing mode, and (c) tearing mode.

The basic tenet of fracture mechanics is that the strength of most real solids is

governed by the presence of flaws and, since the various theories enable the manner in which they propagate under stress to be analyzed mathematically, the application of fracture mechanics to crack growth in polymers has received considerable attention. Two main, interrelatable, conditions for fracture are proposed. First, the energy criterion arising from studies like Griffith (1920), and later Orowan (1948), which suggested that fracture occurs when sufficient energy released from the stress field by growth of the crack to supply the requirements of the new fracture surfaces. The energy released comes from stored elastic or potential energy of the loading system and can, in principle, be calculated for any type of test pieces. This approach, therefore, provides a measure of the energy required to extend a crack over unit area and this is termed the fracture energy or critical strain-energy release rate and is denoted as G_c. Second, Irwin (1964) found that the stress field around a sharp crack in a linear elastic material could be uniquely defined by a parameter named the stress-intensity factor, K_I, and stated that fracture occurs when the value of K_I exceeds some critical value, K_{Ic}. Thus, K_I is a stress field parameter independent of the material whereas K_{Ic}, often referred to as the fracture toughness, is a measure of a material property. The J-integral method suggested by Rice (1968) has received considerable attention. This concept is not only used as criterion of onset of crack propagation, but also used to study propagation stability (Paris 1977). The definition and meaning of the J concept can be considered in different ways: the path integral, the variation of energy with the crack length (Sumpter and Turner, 1976), the factor characterizing the crack type singularity (Hutchinson, 1968). Except for special circumstances (Bilby 1977), the J-integral is path independent only for elastic material (linear or nonlinear). Chan et al (1970) approached a local fitting procedure for

estimating stress intensity factors. Such procedures are long-standing practice in fracture mechanics, predating the early evaluation of their use. The reason why his method is popular is that the method can be reproduced and verified easily. Although the method is not as accurate as path independent method such as the J-integral, it can be used to analyze the composite material for its advantages. The J-integral method is not suitable for the complex material when the anisotropic material is treated as an isotropic material. After the recent survey of the application of finite element methods in linear elastic mechanics by Pang (1993), they continue to be in use today. Generally, local fitting methods match field quantities near the crack tip to infer the participation of the singular fields right at the crack tip. The methods are considered to match asymptotic expressions for crack face displacements with finite element results. Errors thus occurred by the accompanying Finite Element Analysis (FEA) are confined to those associated with displacements. There is the possibility of fitting errors, i.e., errors from the contributions of other nonsingular crack tip fields which are not included in the fit. Recently, Sinclair (1984) showed that path independent integral method can be used to compute stress intensity factors at sharp notches in elastic plates. Santosh and John (1999) studied the three dimensional nature of stress fields in the near tip region of a cracked orthotrophic plate. They found that the size of plane strain zone around the crack tip were highly dependant on the amount of orthotropy and on the Poisson's ratios. Livieri (2001) applied the J-integral to rounded V-notch subjected to mode I loading. He founded that sharp notches are limited in use for rounded notches with linear flanks. Rousseau and Tippur (2002) examined the behavior of the crack tip stress field for functional grade material (FGM) beams subjected to pure bending with an edge crack parallel to the

elastic modulus gradient. They found that a nearly constant fracture toughness in the region where the filler volume fraction is >0.25. More recently, Choi and Sankar (2003) formulated a method to compute fracture toughness of carbon form by the solid and beam model.

3.2 OBJECTIVES

The purpose of this chapter was to provide a numerical model for fracture behavior of wood plastic composite, based on statistical technique and finite element method. In accomplishing this goal, the following specific objectives were met:

1) To develop an experimental procedure to study fracture toughness of wood plastic composite;
2) To simulate the fracture behavior of wood plastic composite using a finite element model; and
3) To validate the model using converging check and patch test

3.3 MATERIALS AND METHODS

3.3.1 Three Point Bending Test

According to the ASTM D790, three point bending tests were conducted for each specimen using an Instron test machine to develop elastic constants for the simulation analysis. Rectangular specimens were placed flat-wise on a test span of 28 cm in order to provide span-to-depth ratio of approximately 16. The modulus of rupture and modulus of elasticity for each specimen are calculated by the following equations:

$$\text{MOR} = 3\text{PL}/2\text{bd}^2 \qquad [3.1]$$

$$\text{MOE} = \frac{P_1 L^3}{48ID} \qquad [3.2]$$

Where:
b = width of specimen (mm)
d = thickness (depth) of specimen (mm)
L = length of span (mm)
P = maximum load (N)
P_1 = load at proportional limit (N)
D = displacement (mm)
I = moment of inertia (mm^4)
MOR = modulus of rupture (kPa)
MOE = modulus of elasticity (GPa)

3.3.2 Four Point Bending Test

In this study, the single edge notched four point bending specimens were used to measure fracture toughness (K_{Ic}). In fact, the four point bending test would yield more accurate and reproducible results as the crack is in the region under constant bending moment and has no transverse shear force. The specimen was cut with a table saw, and a notch was cut using a band saw. Four point bending tests were conducted on an Instron test machine with the span 17.06cm and with the cross head speed of 0.05cm/min.

For a single notch specimen under pure bending and an elastic isotropic material, the fracture toughness is

$$K_{Ic} = \frac{6M}{(w-a)^{3/2}} f(\alpha) \qquad [3.3]$$

Where α =a/W,

Table 3.1. Stress intensity factor coefficients f(a/w) for notched beams (Bodig and Jayne 1982)

a/w	0.05	0.1	0.2	0.3	0.4	0.5	0.6
f(α)	0.36	0.49	0.60	0.66	0.69	0.72	0.73

$$\sigma_O(P)=3P(L-c)/2W^2B \qquad [3.4]$$

Where P (kgf) is the applied load, L (cm) is the distance of two points of bottom supports, c is the distance of two points of applied load, h is the height of the specimen, and b is the width of the specimen.

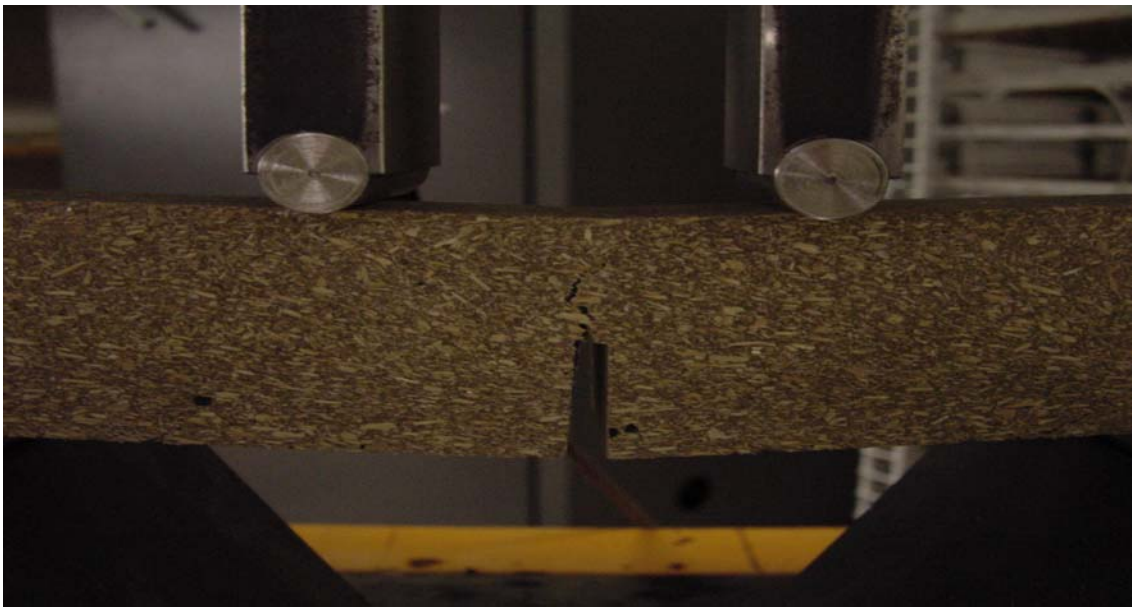

Figure 3.2 Four point bending test showing a failed WPC sample.

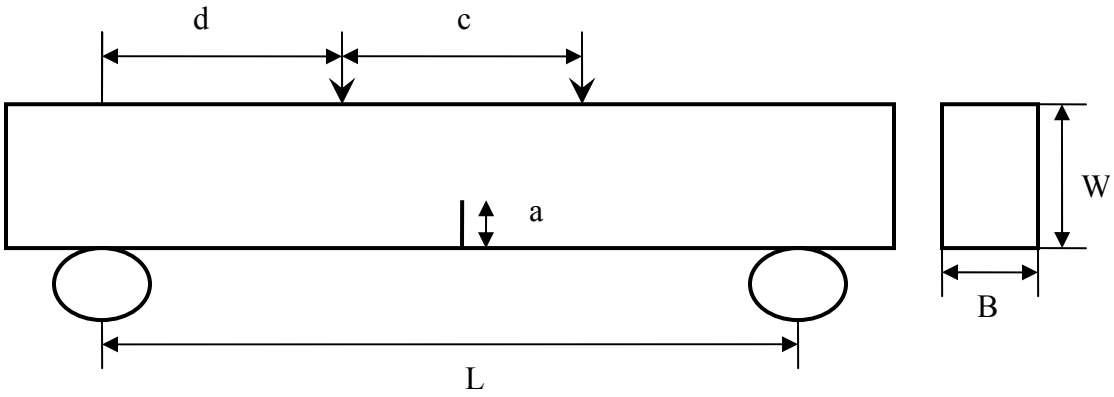

Figure 3.3 Four point bending test diagram with notch length (a=0.76, 0.95, 1.39, and 2.10cm), width (B=3.3cm), distance between applied load (c=5.68cm), distance between bottom support and applied load (d=5.68cm), depth (W=4.06cm), and length of specimen (L=17.6cm)

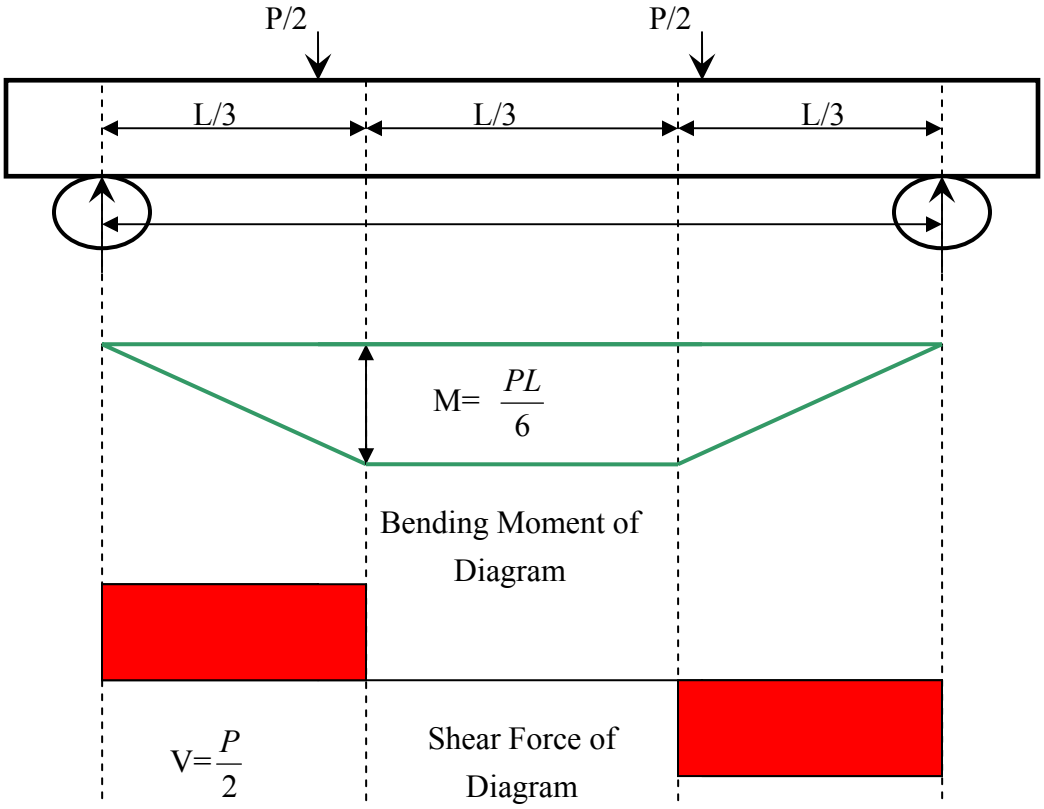

Figure 3.4 Bending moment and shear force diagrams from four point bending tests.

3.4 FEM SIMULATION

3.4.1 Elemental Material Properties

The first step in simulating the fracture behavior of WPC is to idealize the material properties. The measured Young's modulus of WPC was obtained from three-point bending test and density was obtained from X-ray density profile system. A Poisson's ratio of 0.3 was assumed. Theory of linear elastic fracture mechanics (LEFM) was used in this simulation. Thus, WPC was regarded as an isotropy material as a first approximation. An identical elastic constant and density value was used for every element. Also as the material used in the experimental test was thick in thickness, plain strain case with the actual thickness of the specimens was assumed, which means three principle stresses occurs and no dimension shrinkage occur in the thickness direction.

3.4.2 Construction Area of Four Point Bending Simulation

To create the area for the half simulation of the four point bending test, the key point command in ANSYS was used. The location of each key point was defined corresponding to the actual dimension of the four point bending specimen. After the key points were defined, a line command was used to draw lines between the key points. After drawing the lines, the lines were selected to generate the corresponding area (Figure 3.7.a.). To generate the quarter point triangle element around the crack tip, part of area three (A3) near crack tip was first subtracted to create a key point at the crack tip. The Line command was again used to create area five (A5) (Figure 3.7.d.). Glue command was used to connect the each area as one area.

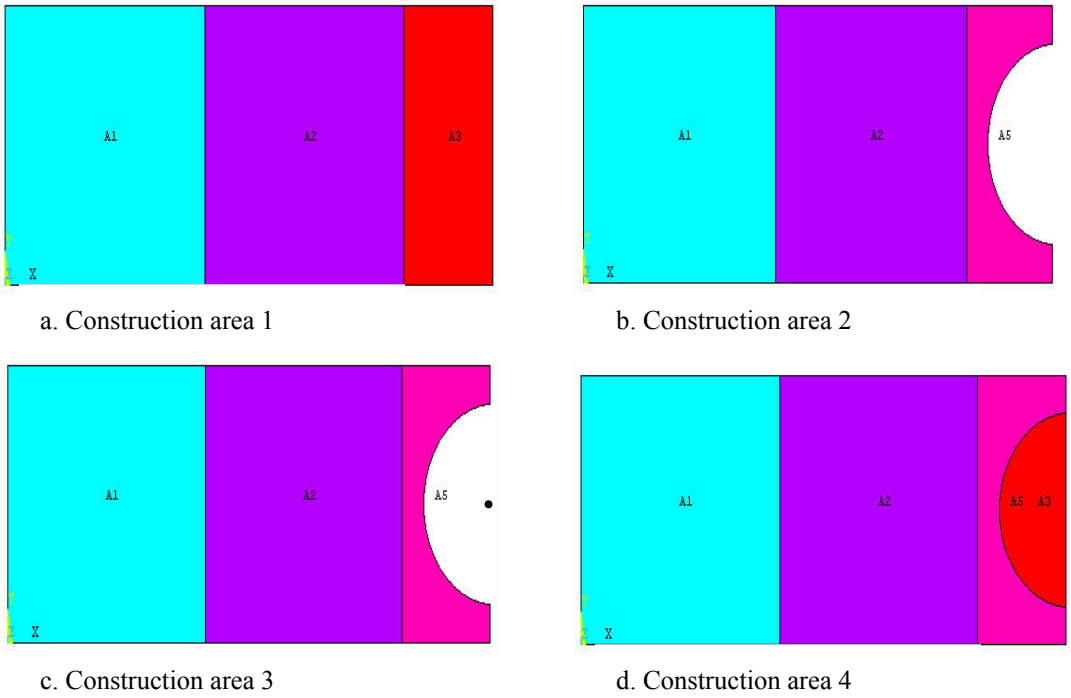

a. Construction area 1

b. Construction area 2

c. Construction area 3

d. Construction area 4

Figure 3.5 Creation of simulation model of four point bending test. Construction area 1 (a), construction area 2 (b), construction area 3 (c), construction area 4 (d).

3.4.3 Quarter Point Elements

An isoparametric element having side nodes can be made to incorporate the desired stress field merely by moving side nodes so they appear at quarter points rather than at midsides (Figure 3.6). The following equations (3.5) and (3.6) are obtained by shape functions (Sills 1991):

$$\xi = 2\sqrt{\frac{x}{l}} - 1 \qquad [3.5]$$

$$\varepsilon_x = \left[\left(\frac{2}{l} - \frac{3}{2\sqrt{lx}}\right)\left(\frac{4}{-l} + \frac{2}{\sqrt{lx}}\right)\left(\frac{2}{l} - \frac{1}{2\sqrt{lx}}\right)\right]\begin{Bmatrix} u_1 \\ u_2 \\ u_3 \end{Bmatrix} \qquad [3.6]$$

Equation (3.6) shows that if x <<l, then ε_x varies inversely with $\sqrt{x}$ implying that the desired singularity is present. The element retains the ability to represent rigid body motion without strain, and the ability to represent a constant strain state.

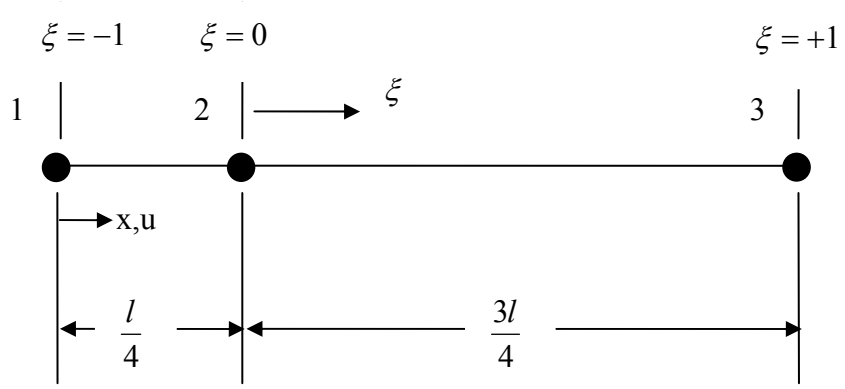

Figure 3.6 Quarter point nodes for linear singularity

Six-node triangles behave the same way. Therefore, it is appropriate to surround a crack tip by a dislike patch in which element sides emanating from the crack tip have their nodes at quarter points, as shown in Figure 3.9. In this study, among the element types provided by the ANSYS, plane-82 element was used for 2-D fracture mechanics analysis. Around the crack tip 6 triangle elements with $\alpha = 30^0$ were used and 8 quad elements were used for the rest area. A triangle element length was a/4, a/8, a/16, a/32 for coarse, medium, fine, super fine grid respectively (Figure 3.7). The number of different element for four girds is summarized in Table 3.2.

Table 3.2 The sequence of four elements for finite element analysis on four point bending test.

Grid	8 quad element	6 triangle element	Total element
Coarse	213	12	225
Medium	237	15	242
Fine	240	15	255
Super Fine	250	18	268

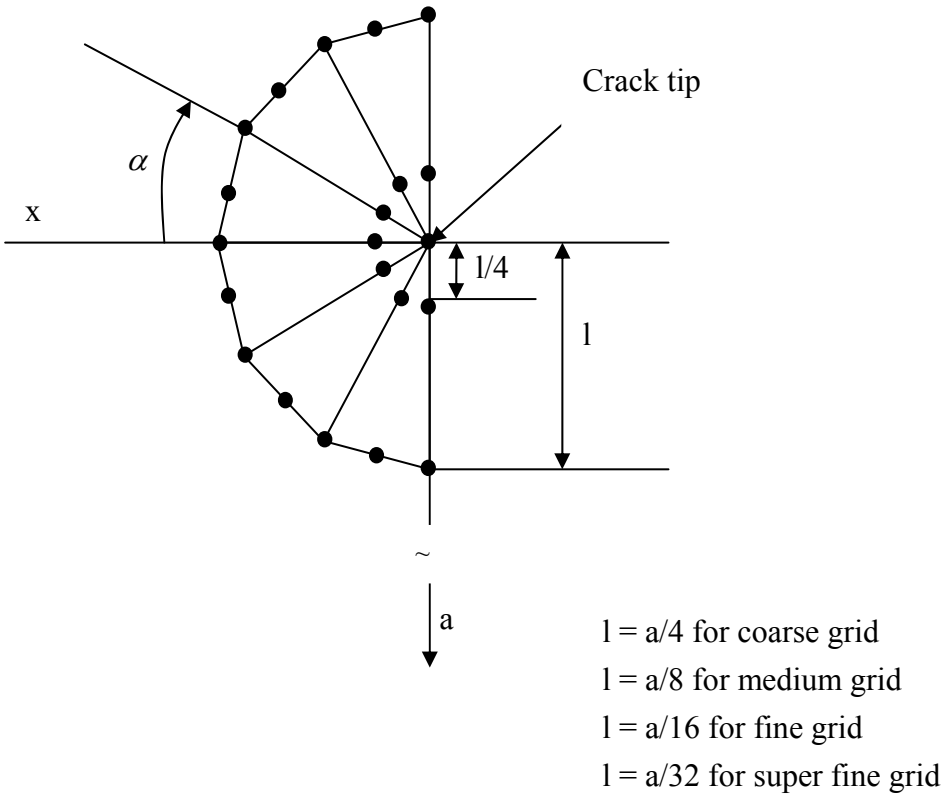

Figure 3.7 Quarter point triangle elements generated disk-like patch mesh around crack tip.

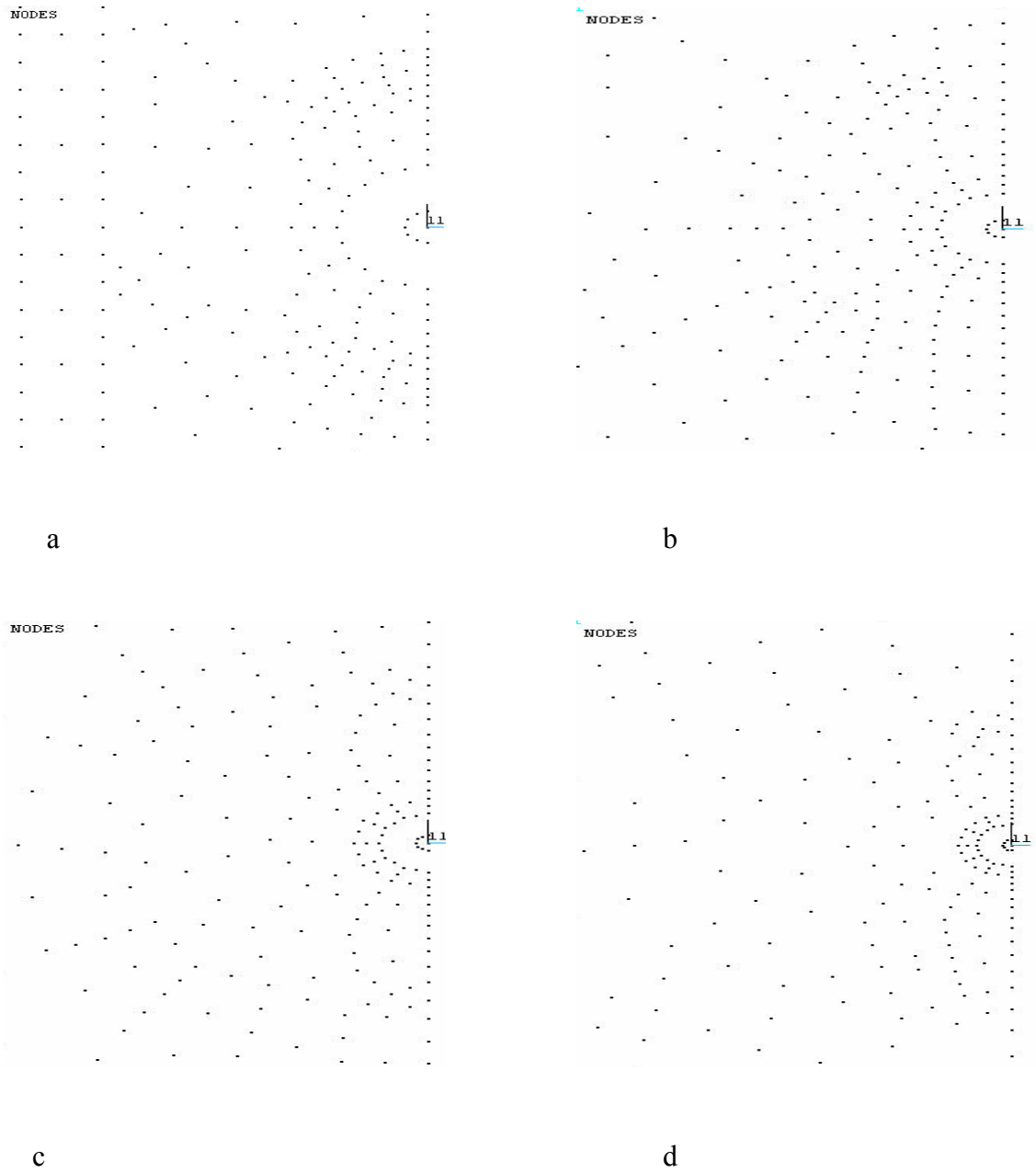

a b

c d

Figure 3.8 Local coordinates at the crack tip for computing stress intensity factor. (a) coarse node around crack tip , (b) medium node around crack tip, (c) fine node around crack tip, and (d) super fine node around the crack tip.

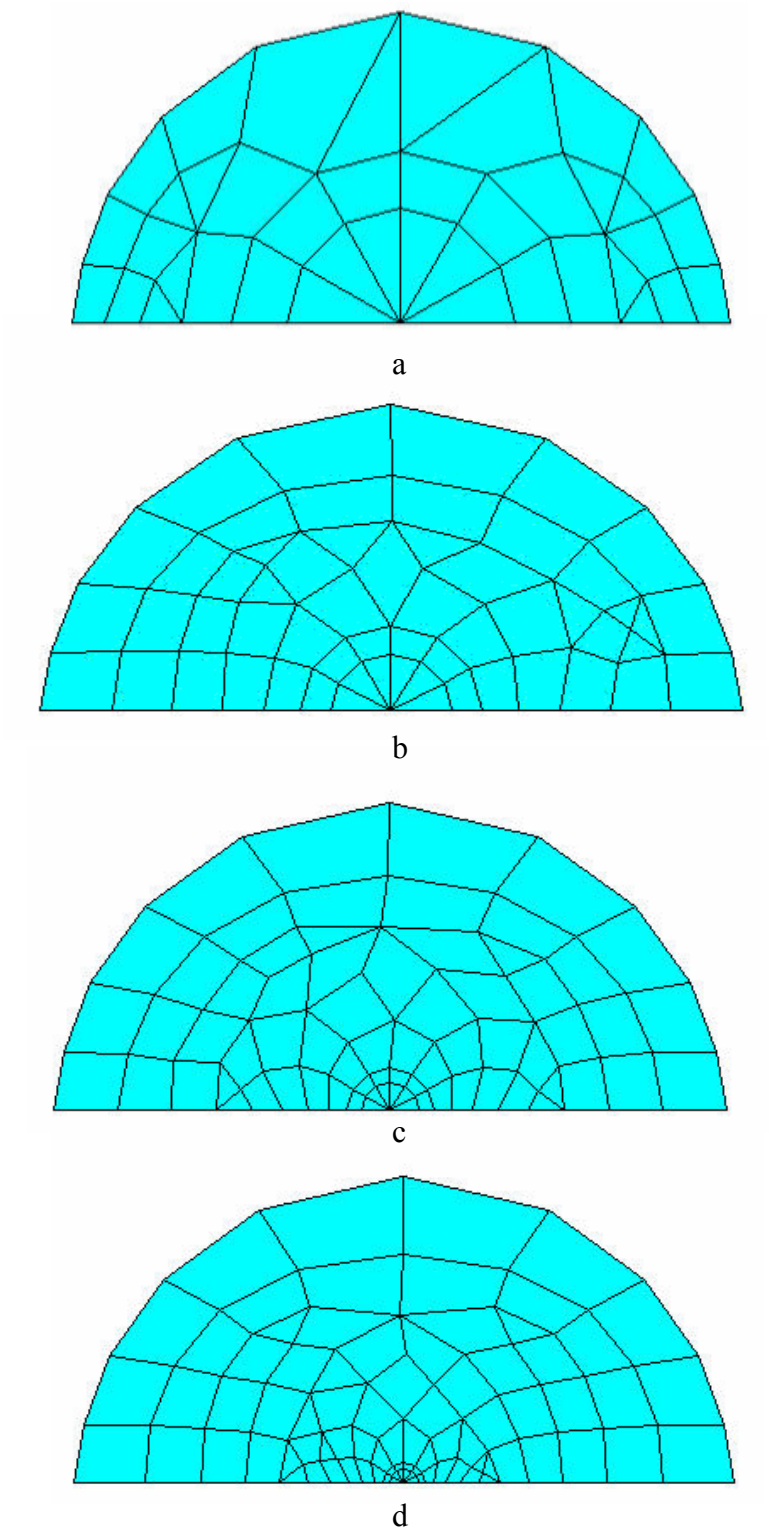

Figure 3.9 Meshing around the crack tip. (a) coarse mesh, (b) medium mesh, (c) fine mesh, and (d) super fine mesh.

3.4.4 Boundary Condition and Field Equations

Because of symmetry condition, only half of the four point bending specimen was simulated in FEM (Figure 3.10). Displacement boundary conditions and loading conditions were applied to the region ($\Re$) based on linear elastic fracture mechanics (LEFM) for isotropic materials.

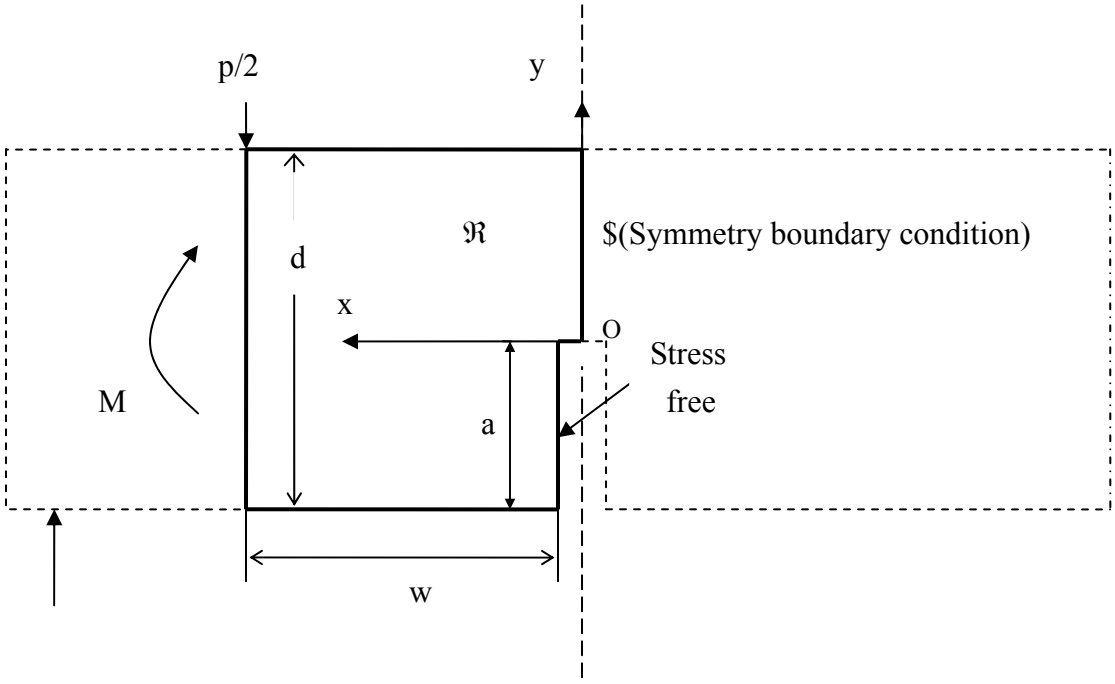

Figure 3.10 Boundary condition for finite element analysis with M for bending moment, p for applied load, and a for length of crack.

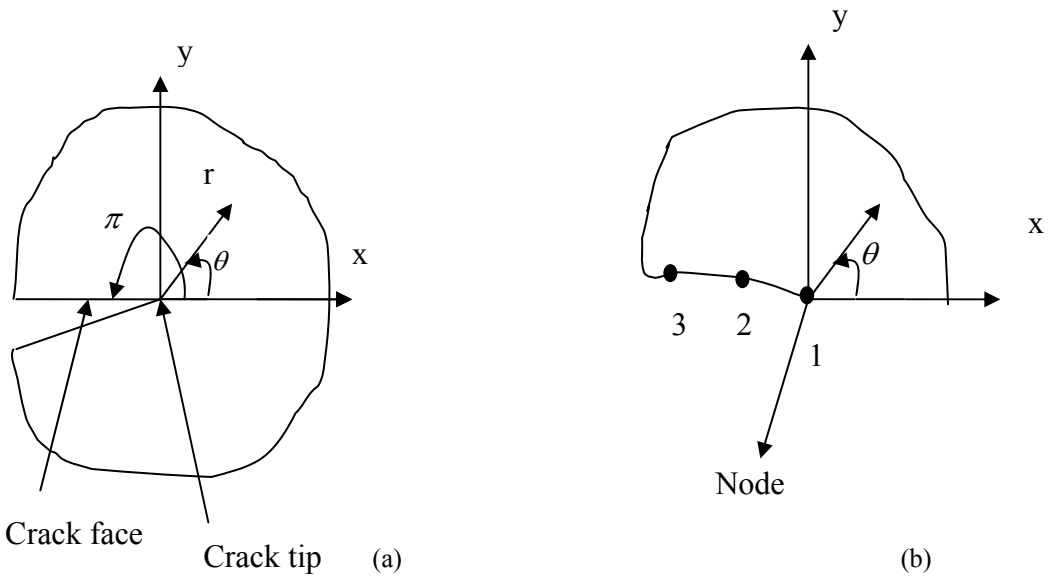

Figure 3.11 Polar coordinate model around crack tip with local coordinate system at crack tip (a) and path definition for three nodes (b).

In analyzing stress intensity factor, region (R) is the area of interest

$$\Re = \{(x,y) \mid 0 < x < w, \quad -a < y < d-a\}$$

And the governing boundary conditions are as follows. The applied moment condition for –a < y < d-a is

$$\sigma_x = \frac{6M}{d^2}\left[1 - \frac{2}{w}(y+a)\right] \qquad \tau_{xy} = 0 \quad \text{on x = w} \qquad [3.7]$$

The stress-free crack conditions for –a < y < 0 are

$$\sigma_x = 0\,, \quad \tau_{xy} = 0 \quad \text{on x} = 0 \qquad [3.8]$$

The symmetry conditions for 0 < y < d-a are

$$\tau_{xy} = 0\,, \text{ u=0 x} = 0 \qquad [3.9]$$

The stress-free conditions on the front and back edges for 0 < x < w

$$\sigma_y = \tau_{xy} = 0 \quad \text{on y = -a, d-a} \qquad [3.10]$$

To calculate stress intensity factor K_I, a local crack tip coordinate system was defined as x parallel to the crack face and y perpendicular to the crack face, and three nodes along the path from the tip were chosen as shown in the Figure 3.11a and b. Turning attention to a polar coordinate system, the symmetry of the x-axis was confined to be the region R in Figure 3.11a.

$$R= \{ (r,\theta) | 0 < r < a,\ \ 0 < \theta < \pi \}.$$

In the region, the stress and displacements are represented by functions of r and θ and denoted below. The stress equations of equilibrium, in the absence of body forces, require

$$\begin{aligned} &r\sigma_{r,r} + \tau_{r\theta,\theta} + \sigma_r - \sigma_\theta = 0, \\ &\sigma_{\theta,\theta} + r\tau_{r\theta,r} + 2\tau_{r\theta} = 0, \end{aligned} \qquad \text{on R} \qquad [3.11]$$

where subscripts proceeded by a comma denote differentiation with respect to that variable. In terms of the polar coordinates r and θ for opening mode crack surface displacements, the governing field equations (3.11) can be interpreted as Equations (3.12) and (3.13) respectively:

$$\frac{\partial \sigma_r}{\partial r} + \frac{1}{r}\frac{\partial \tau_{r\theta}}{\partial \theta} + \frac{\sigma_r - \sigma_\theta}{r} = 0 \qquad [3.12]$$

$$\frac{1}{r}\frac{\partial \sigma_\theta}{\partial \theta} + \frac{\partial \tau_{r\theta}}{\partial r} + \frac{\partial \tau_{r\theta}}{r} = 0 \qquad [3.13]$$

$$\nabla^2(\sigma_r + \sigma_\theta) = 0 \qquad [3.14]$$

Equation (3.12) and Equation (3.13) are called equilibrium equations in polar coordinates. Those two equations could be derived using Taylor expansion like the equilibrium equations in Cartesian coordinates. Equation (3.14) is a compatibility equation. From Equation (3.14), the following Equation (3.15) is derived using separate variables:

$$\sigma_r + \sigma_\theta = r^\lambda (a\cos\lambda\theta + b\sin\lambda\theta) \qquad [3.15]$$

The plane-strain stress-displacement relations, for an isotropic linear elastic material, require

$$\begin{aligned} \sigma_r &= 2G(1-2\nu)^{-1}\left[(1-\nu)u_{r,r} + \nu r^{-1}\left(u_r + u_{\theta,\theta}\right)\right] \\ \sigma_\theta &= 2G(1-2\nu)^{-1}\left[(1-\nu)r^{-1}\left(u_r + u_{\theta,\theta}\right) + \nu u_{r,r}\right] \\ \tau_{r\theta} &= G\left[u_{\theta,r} + r^{-1}\left(u_{r,\theta} - u_\theta\right)\right] \end{aligned} \qquad [3.16]$$

In Equation (3.16), G is shear modulus and Poison's ratio equals to 0.3.

$$\begin{aligned} \sigma_r &= \frac{1}{2}G\left[7u_{r,r} + 3r^{-1}(u_r + u_{\theta,\theta})\right] \\ \sigma_\theta &= \frac{1}{2}G\left[7r^{-1}(u_r + u_{\theta,\theta}) + 3u_{r,r}\right] \\ \tau_{r\theta} &= G\left[u_{\theta,r} + r^{-1}(u_{r,\theta} - u_\theta)\right] \end{aligned} \qquad [3.17]$$

The symmetry conditions ahead of the crack is

$$u_\theta = 0, \quad \tau_{r\theta} = 0, \quad \text{on} \quad \theta = 0 \quad (0<r<a) \qquad [3.18]$$

The stress free crack face condition is

$$\sigma_\theta = 0, \quad \tau_{r\theta} = 0, \quad \text{on} \quad \theta = \phi \quad (0<r<a) \qquad [3.19]$$

, while the traction and displacement conditions separately require, respectively

$$\sigma_r = \sigma_r^I, \quad \tau_{r\theta} = \tau_{r\theta}^I \qquad \text{on r = a} \qquad [3.20]$$

$$u_r = u_r^I, \quad u_\theta = u_\theta^I \qquad \text{on r = a} \qquad [3.21]$$

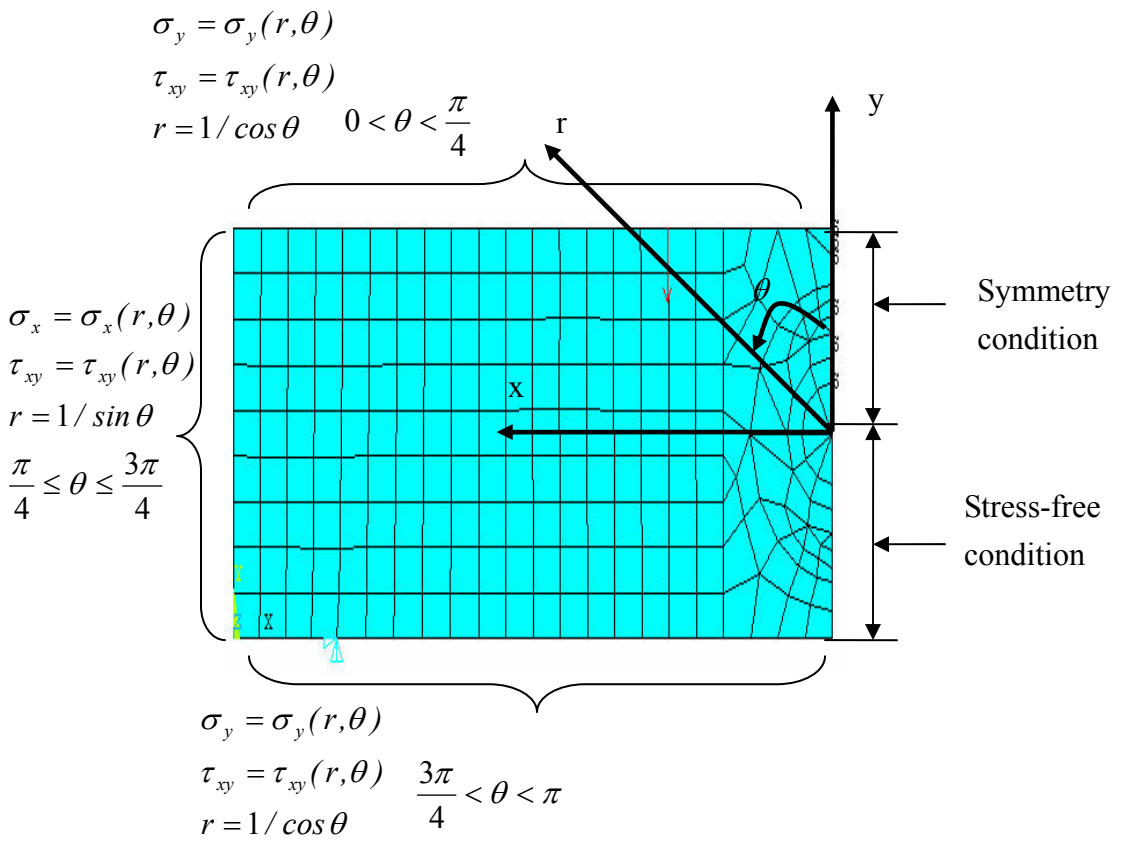

Figure 3.12 Symmetric boundary conditions and loading conditions from four point bending simulation.

Since the four point bending specimens are under symmetric loading having resultant force per unit thickness, applied load (p) acting transverse to the crack is assumed. Then the only stress intensity factor present is the mode I case. Focusing on the boundary conditions (Equation 3.18-3.21), Equation (3.15) is transformed to the following Equation (3.22):

$$\sigma_r = r^{\lambda}\left[(2-\lambda)c_1 \cos\lambda\theta - c_2 \cos(\lambda+2)\theta\right]$$

$$\sigma_\theta = r^{\lambda}\left[(2+\lambda)c_1 \cos\lambda\theta + c_2 \cos(\lambda+2)\theta\right] \quad [3.22]$$

$$\tau_{r\theta} = r^{\lambda}\left[\lambda c_1 \sin\lambda\theta + c_2 \sin(\lambda+2)\theta\right]$$

To have a solution for Equation (3.22), the determinant of either σ_r and $\tau_{r\theta}$ or σ_θ and $\tau_{r\theta}$ is equaled to 0. Therefore, eigen-value equation for crack is:

$$(\lambda+1)\sin 2\theta + \sin 2(\lambda+1)\theta = 0 \quad [3.23]$$

In this study, the angle between symmetry condition and stress free condition is 180°

For this problem, $\theta = \pi$

$$\sin 2(\lambda+1)\pi = 0 \quad [3.24]$$

λ = -1/2, 0, 1/2 (Eigen-values)

Sustituting -1/2 for λ to Equation 24, the crack problem with $\theta = \pi$ for the stress equations in polar coordinated are derived as,

$$\sigma_r = \frac{c_2}{\sqrt{r}}\left[5\cos\frac{\theta}{2} - \cos\frac{3\theta}{2}\right]$$

$$\sigma_\theta = \frac{c_2}{\sqrt{r}}\left[3\cos\frac{\theta}{2} + \cos\frac{3\theta}{2}\right] \quad [3.25]$$

$$\tau_{r\theta} = \frac{c_2}{\sqrt{r}}\left[\sin\frac{\theta}{2} + \sin\frac{3\theta}{2}\right]$$

From Equation (3.25), γ must be such that σ meets the singularity requirements

which induce that

$$\sigma_{ij} = o\left(\frac{1}{r^{\lambda+1}}\right) \qquad , \quad o \text{ = order} \qquad [3.26]$$

To define mode I stress intensity factor (K_I), the following equations can be introduced:

$$K = \sigma_{ij}\sqrt{2\pi r} / f_{ij}(\theta) \qquad [3.27]$$

$$\begin{Bmatrix} \sigma_{11} \\ \sigma_{12} \\ \sigma_{22} \end{Bmatrix} = \frac{K_I}{\sqrt{2\pi r}} \cos(\theta/2) \begin{Bmatrix} 1+\sin(\theta/2)\sin(3\theta/2) \\ \sin(\theta/2)\cos(3\theta/2) \\ 1-\sin(\theta/2)\sin(3\theta/2) \end{Bmatrix} \qquad [3.28]$$

For plane strain,

$$\sigma_{33} = \nu(\sigma_{11} + \sigma_{22}) \qquad [3.29]$$

$$\sigma_{23} = \sigma_{13} = 0 \qquad [3.30]$$

Only the first term of Equation 3.28 is shown. The complete equations are power series in r/a (crack tip radius/crack half-length). For practical purposes, all terms beyond the first are negligible. All the three stress components (σ_{11}, σ_{12}, and σ_{22}) are proportional to a scalar quantity that has been designated the stress intensity factor, K_I. This factor is independent of r and θ and therefore gives a single description of the stress intensity at any point near the crack tip. It is a purely numerical quantity which, if known, provides a complete knowledge of the stress field at the crack tip. Local fitting method was used for stress intensity factor of WPC. Stress values at the crack tip were obtained and then stress intensity factors were evaluated.

3.5 RESULTS AND DISCUSSION

3.5.1 Three Point Bending Test Result

To determine the elastic constants of WPC in two fiber orientations, three point bending test was carried out. The mean value of peak load, MOR, and MOE of WPC for perpendicular direction specimen are 114.1 (kgf), 11.8 (MPa), and 1.12 (GPa) respectively. The mean value of peak load, MOR, and MOE for the parallel direction specimens are 76.37 (kgf), 8.4 (MPa), and 0.69 (GPa) respectively. From these results, we can expect that when the load is in the direction parallel to the fiber orientation, WPC will give poor performance mechanically compared to when the load applied to the perpendicular to the direction of the fiber orientation.

Table 3.3 Three point bending test with mean value of actual dimension and mechanical properties with w for width of the specimen, d for depth of the specimen, and l for length of the specimen (the direction of fiber parallel to the load head).

Parallel direction to the load head								
	w (mm)	d (mm)	l (mm)	span (mm)	Peak Load (kgf)	MOR (MPa)	MOE (GPa)	M.C (%)
Mean	77.3	17.4	304.8	280	151.9	16.7	1.38	0.07
S.T.D	0.002	0.001	<.0001	280	0.85	0.10	0.01	0.2

Table 3.4 Three point bending test with mean value of actual dimension and mechanical properties with w for width of the specimen, d for depth of the specimen, and l for length of the specimen (the direction of fiber perpendicular to the load head).

Perpendicular direction to the load head								
	w (mm)	d (mm)	l (mm)	span (mm)	Peak Load (kgf)	MOR (MPa)	MOE (GPa)	M.C (%)
Mean	7.73	1.75	30.48	280	222.1	23.6	2.23	0.07
S.T.D	0.003	0	<.0001	280	6.11	0.18	0.02	0.5

* S.T.D – standard error

3.5.2 Four Point Bending Test Result

Four point bending tests with four different notch lengths showed that peak load and modulus of rupture (MOR) were increased as notch length decreased (Figure 3.14). Compared to MOR of sample R, which had no flaw geometry, MOR of the sample A which had 0.5 in a ratio of notch length to depth decreased almost 80%. Fracture toughness of WPC was slightly changed by the variation of notch length in specimens A, B, and C. However, the fracture toughness of specimen D was 7% lower than the mean value of the rest three groups (Figure 3.13). Fracture toughness represents the material property that the crack occurs when the load is higher than the material resistance of initiating the crack, while stress intensity factor shows elastic stress field around the crack tip when the load is applied to the material. Thus, the two can be differentiated as strength and stress respectively. Therefore, it can be assumed that fracture toughness is independent of notch length. The reason why the specimen D had substantially lower fracture toughness was assumed to be that WPC has anisotropic properties which occur by different directions of fibers, porous, interfacial area, and different proportion of fibers and polymer within the material. Because the specimen D had short length of notch, it had more area of material than the rest three groups, which means it could be more affected by the complex properties. Therefore, it can be concluded that fracture toughness of WPC is 1.79 MPa$\sqrt{m}$ which is quite higher than that of most of the solid wood. The average fracture toughness of solid wood was found to be 0.3 MPa$\sqrt{m}$. Yellow-poplar had the highest fracture toughness of 0.51 MPa$\sqrt{m}$ in mode I fracture (wood handbook 1991). However, WPC are still needed to improve the fracture toughness to compete with metals of which fracture toughness has over 100 MPa$\sqrt{m}$.

Table 3.5 Four point bending results with mean value of actual specimen dimension and fracture toughness (Mode I).

Sample	Notch Length (mm)	Width (mm)	Depth (mm)	Length (mm)	Span (mm)	Density (kg/m^3)	Peak Load (kgf)	MOR (MPa)	Fracture Toughness ($MPa\sqrt{m}$)
R	0	35	40.9	176	232	1107.2	766.5	21.8	
A	21.1	33.2	42.1	176	232	1107.2	156.0	4.4	1.846
B	13.9	32.7	42.1	176	232	1107.2	243.7	7.0	1.758
C	9.5	33	38.1	176	232	1107.2	269.3	9.4	1.780
D	7.6	33	38.1	176	232	1107.2	292.6	10.2	1.670

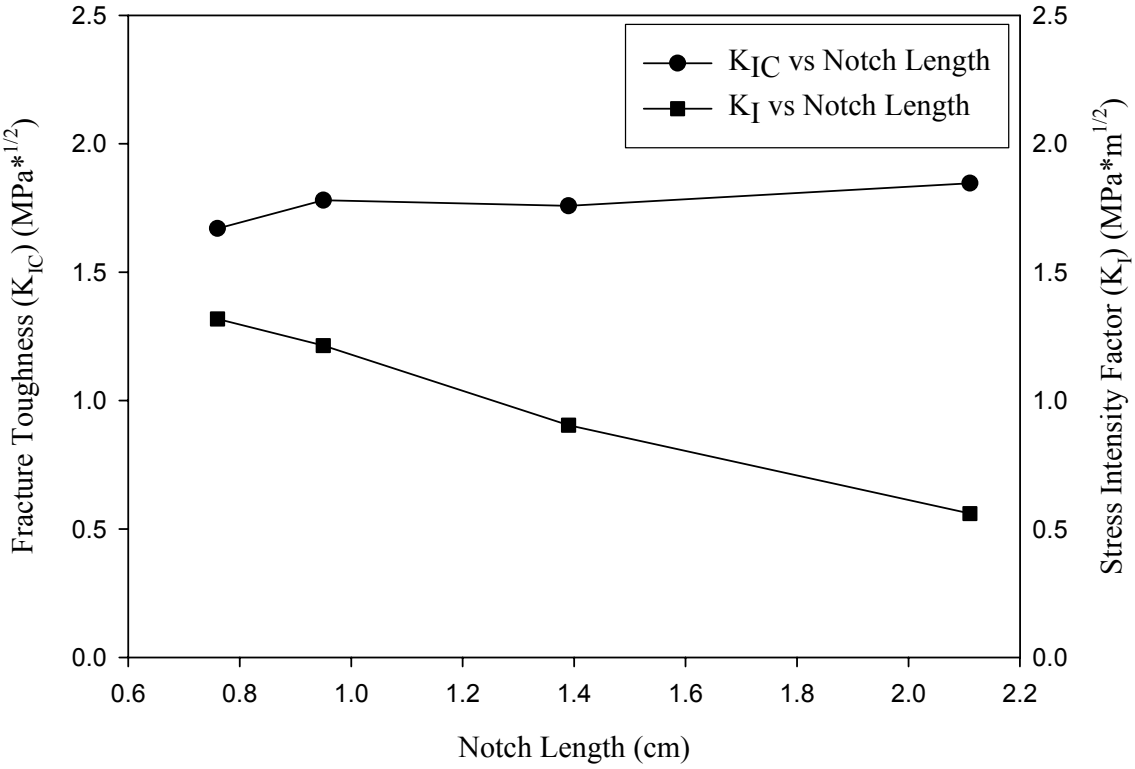

Figure 3.13 The effect of notch length on stress intensity factor and Fracture toughness of WPC by four point bending tests.

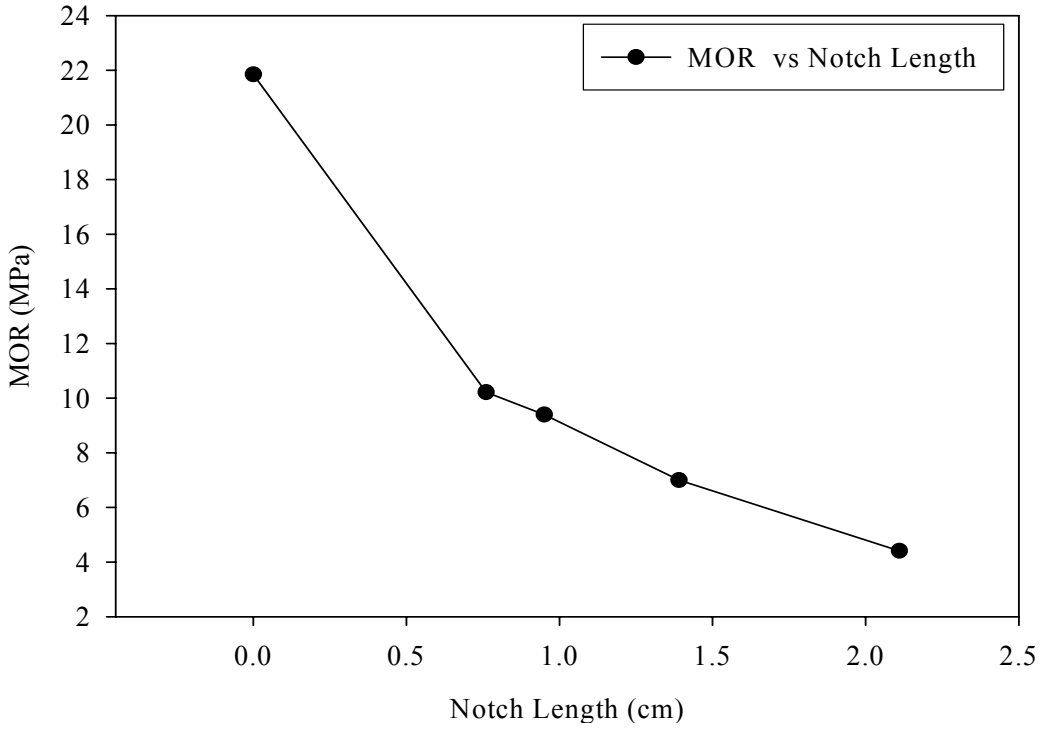

Figure 3.14 The effect of notch length on modulus of rupture of WPC by four point bending tests.

3.5.3 Finite Element Analysis Result

Linear elastic stress concentrations found near notch roots or crack tips can degenerate upon crack initiation into an infinite stress singularity, and crack propagation, therefore, has to be based on stress intensity factors or other energetic parameters rather than on the magnitude of stress itself, which is not bounded (Figure 3.15). The stress intensity factor was calculated by means of the ANSYS KCALC command, which is based on an algorithm that uses the displacements around the tip of the crack. For this purpose, the elements of the first row around the tip of the crack were modified by displacing the mid-side nodes at the quarter point from the tip. The results are summarized in Table 3.6. As the meshes were refined progressively from coarse grid to

super fine grid, the stress of σ_x, σ_y, principal stress1, and principal stress2 were diverged at the crack tip. Stress intensity factor, however, was converged to 568.56 (kPa$\sqrt{m}$). From the finite element results, the mode I stress intensity factor that will cause failure of a crack tip element was determined and it was taken as the predicted failure toughness of the WPC. Crack propagation before failure can be estimated from stress intensity factor (K_I) associated with fracture toughness from the experimental results of the four point bending test. In this study, fracture toughness of WPC was evaluated to 1.79 MPa$\sqrt{m}$. Substituting this numerical value to the following equation,

$$\frac{K_{IC}}{K_I} = 3.14 \qquad [3.29]$$

Since the length of position vector (r) from super fine grid was 0.16mm, failure occurs when crack propagates 0.5mm from the crack tip.

Table 3.6 The result of four point bending simulations (Global coordinates)

Grid	σ_x	σ_y	σ_1	σ_2	Stress intensity factor K_I (kPa$\sqrt{m}$)
Coarse	6.72	6.70	7.69	5.73	595.05
Medium	9.26	8.51	10.37	7.40	579.46
Fine	12.92	11.01	14.24	9.69	571.66
Super Fine	18.18	14.52	19.80	12.89	568.56

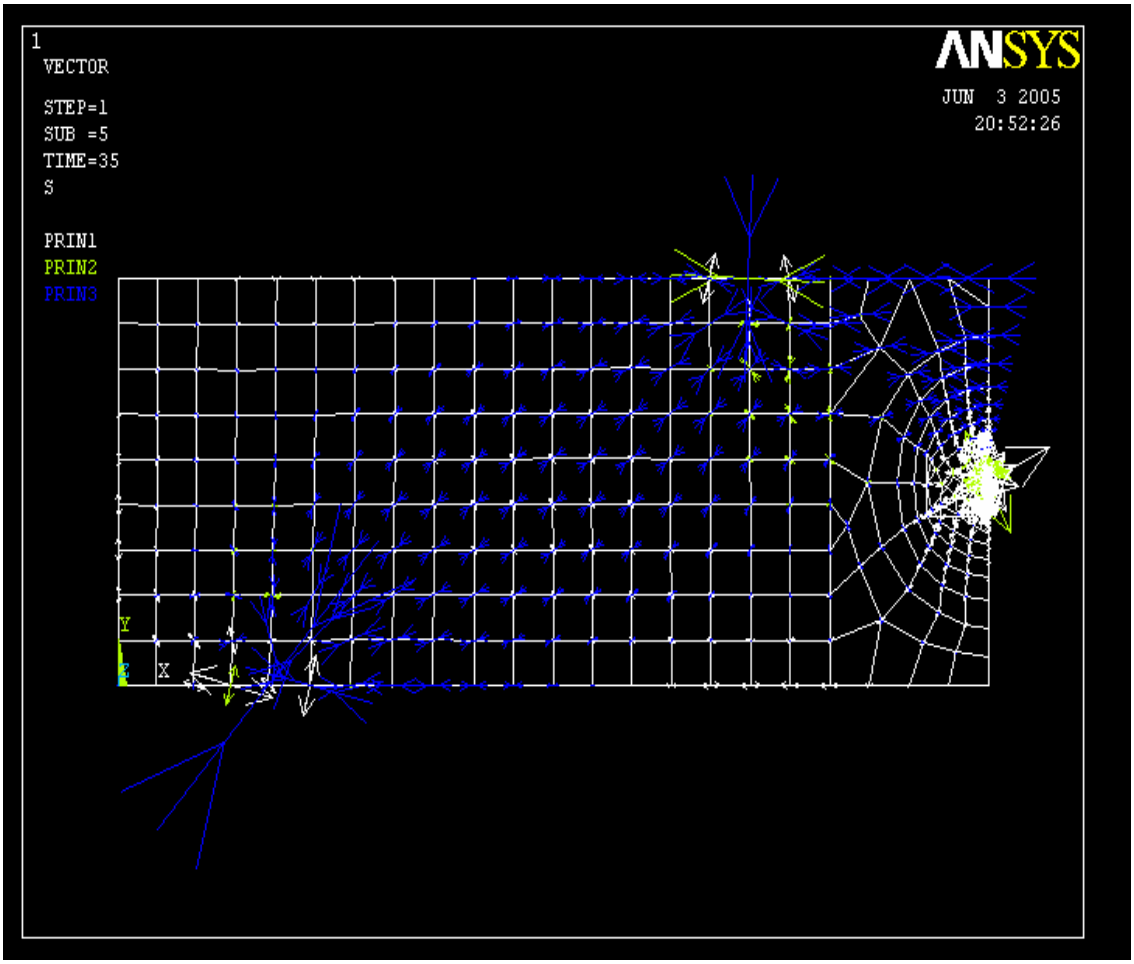

Figure 3.15 Vector contour plot shows the elements, nodes and three principle stresses from ANSYS (finite element analysis software).

3.6 SIMULATION VERIFICATION

In numerical analysis, the two common errors are discretization error and blunder error. First, to check discretization error, four systematic mesh sequences were conducted to check divergence of normal stresses at the crack tip and convergence of stress intensity factor (Table 3.7). Second, in general, there are many different sources that cause blunder errors. In this study, blunder errors were controlled by the comparison of the results from hand calculation with the result from the simulation. Also by the

references (Wood Handbook 1999), the blunder errors were checked. Patch tests were performed to check the continuity of elements in the simulation model (Figure 3.16). For the crack problem, strength of singularity near crack tip should be checked by mathematical formulations (Equation 3.31).

Converging check for stress intensity factor are shown below

$$\left|K_{Ic} - K_{\mathrm{Im}}\right| > \left|K_{\mathrm{Im}} - K_{If}\right| > \left|K_{If} - K_{Isf}\right| \qquad [3.30]$$

$$= 15.59 > 7.8 > 3.1$$

Where,

K_{IC} : stress intensity factor in coarse grid K_{IM} : stress intensity factor in medium grid

K_{IF} : stress intensity factor in fine grid K_{ISF} : stress intensity factor in super fine grid

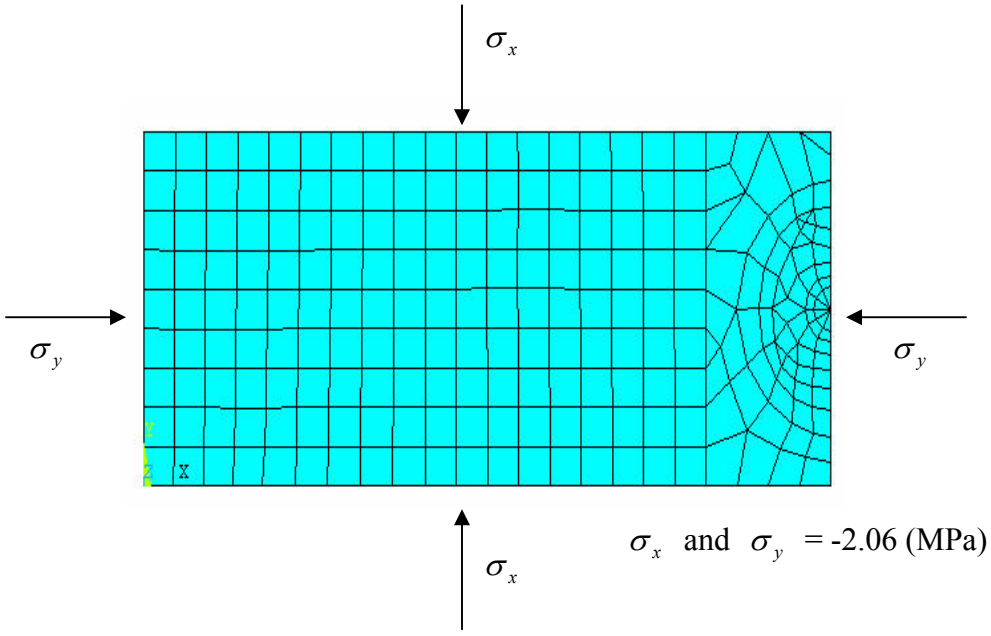

Figure 3.16 Patch test to check the connectivity of the elements.

The result showed that everywhere in the model normal stress equaled to -2.06 (MPa) and parallel (shear) stress equaled to zero.

Estimation of power of singularity at the crack tip was done using:

$$\gamma = \frac{\ln \sigma_x^m / \sigma_x^c}{\ln 2}$$
$$\gamma = \frac{\ln \sigma_x^f / \sigma_x^m}{\ln 2} \qquad [3.31]$$
$$\gamma = \frac{\ln \sigma_x^{sf} / \sigma_x^f}{\ln 2}$$

Where, σ_x^c : normal stress(x) in coarse grid. σ_x^m : normal stress(x) in medium grid

σ_x^f : normal stress(x) in fine grid. σ_x^{sf} : normal stress(x) in super fine grid

The results of power of singularity from the four point bending simulation are summarized in Table 3.7.

Table 3.7 Converging check of normal stress and strength of singularity at the crack tip (Global Coordinates)

Grid	Converging check		Power of the singularity(γ)	
	Δ(Sx)	Δ(Sy)	Sx	Sy
Coarse				
Medium	2.54	1.81	.462	.345
Fine	3.66	2.5	.480	.371
Super fine	5.26	3.51	.492	.399
	Diverging	Diverging	.492	.399
Exact answer	Diverging	Diverging	.5	.5

From William (1950), the order of the singularity for a crack with stress free face for different crack opening angles (COA), if $\sigma = O(r^{-\gamma})$ as $r \to 0$, then k for varying COA is as in Table 3.8.

Table 3.8 Relationship between singularity and crack opening angle (COA) in a linear elastic material

γ	.5	.4999	.4996	.4985	.4965	.4931	.4878	.4801	.4696
COA	0^o	10^o	20^o	30^o	40^o	50^o	60^o	70^o	80^o

A COA generates an expression for inverse square root stress singularity and for a finite energy release rate. From the result of the four point bending simulation by finite element method, strength of singularity of WPC was estimated to 4.92. Therefore, according to the Table 3.8, the crack opening angle (COA) of WPC is approximately 50° in four point bending tests (Figure 3.17).

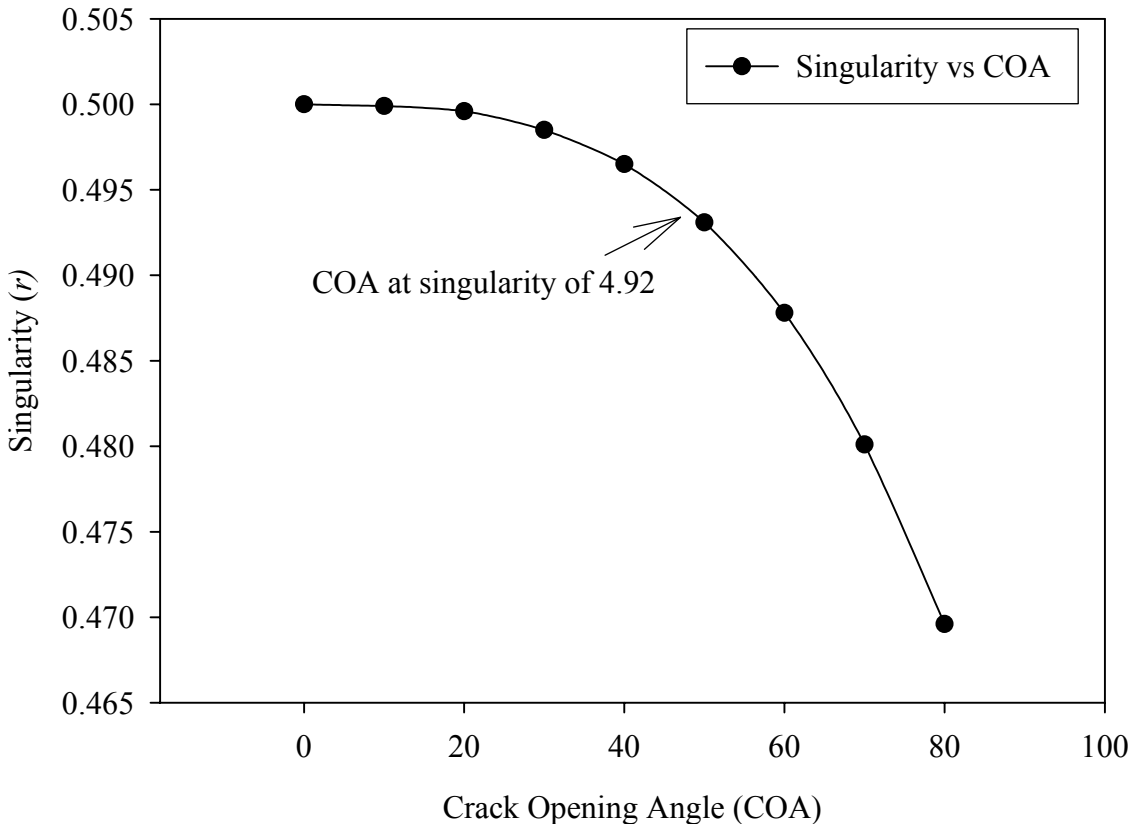

Figure 3.17 Crack opening angle (COA) estimated by strength of singularity.

3.7 CONCLUSIONS

To analyze the fracture behavior of WPC, both experimental test and numerical method were employed. The results of the four point bending test showed that notch length was an inverse function of modulus of rupture and peak load. Fracture toughness of WPC was evaluated as 1.79 (MPa$\sqrt{m}$). The result of this exploratory investigation indicates that there are inherent difficulties in using fracture toughness testing to determine the fracture properties of fiber reinforced polymer. This is due to the very nature of complex matrices, the presence of fibers and the failure behavior of the composite, which are dependant on reinforcing parameters such as portion of fibers, polymers, porous, direction of fibers, and interfacial area. There are increasing needs to identify the most appropriate method to evaluate the fracture toughness of WPC.

A generalized analysis of local fitting methods for stress intensity factor determination using finite element method was outlined. A discussion of the verification of the simulation was also shown. While fracture toughness of WPC is independent of notch length, stress intensity factor was a function of crack length.

The methodology used in this study suggests models to evaluate fracture toughness and stress intensity factor of WPC. It can also be used to develop more advanced models considering nonlinear fracture behavior to predict more accurately the mechanical and physical properties of WPC in future research.

3.8 REFERENCES

Brown, W. F. Jr. and J. E. Srawley. 1966. Plane strain crack toughness of high strength metallic materials, ASTM STP 410, American Society for Testing and Materials.

Jozsef B. and Benjamin A. J. 1982. Mechanics of Wood and Wood composites. 87-176 pp.

Choi, S. and Sankar B. V. 2003. Fracture toughness of carbon foam. J. Comp. Mat. 37:2101-2117.

ANSYS. 2003. ANSYS 8.0 help document, chapter 12. Fracture mechanics.

Rousseau, C. E. and H. V. Tippur. 2002. Evaluation of crack tip fields and stress intensity factors in functionally graded elastic materials: Cracks parallel to elastic gradient. I. J. F. 114: 87-111.

Cooper, D. B., Meda, G., and G.. B. Sinclair. 1995. A comparison of crack-flank displacement fitting for estimating K with a path independent integral. I. J. F. 70: 237-251

Williams, M. L., Pasadena and Calif 1950. Stress singularities resulting from various boundary conditions in angular corners of plates in extension. J. Appl. Mech. 526-528.

Sinclair, G.. B.1980. On the stress singularity at an interface crack. I. J. F. 16:111-119.

Charless, W. F. 1974. Fracture toughness of a rigid polyurethane foam. I. J. F. 10:99-108.

Sinclair, G. B., M. Okajima, and J. H. Griffin 1984. Path independent integrals for computing stress intensity factors at sharp notches in elastic plates. I. J. Num. Met. Eng. 20:999-1008.

Putatunda, S. K. 1986. A comparison of various fracture toughness testing methods. Eng. F. Mech. 25:429-439.

Santosh, P. and John L. 1999. A numerical investigation of three dimensional effects in cracked orthotrophic plates. J. Comp. Mat. 34(2):116-133

Sinclair, G. B. 1985. Some inherently unreliable practices in present day fracture mechanics. I. J. F. 28:3-16.

Sinclair, G. B. 2000. Logarithmic stress singularities resulting from various boundary conditions in angular corners of plates under bending. J. Appl. Mech. 219-223.

Carlos, C. F. 2001. Implementation of domain integral approach for J integral evaluations. Transactions. Smirt 16. Washington DC.

Sills, L. B. 1991. Application of the finite element method to linear elastic fracture mechanics. ASME Appl. Mech. Reviews 44(10):447-461

Francois, D. 1982. Advances in fracture research. 87-94, 97-113, 115-130, 131-139, 141-150. pp.

Willams, J. G.. 1984. Fracture mechanics of polymers. Halsted Press, New York. 22-122 pp.

Kinloch, A. J. and Young R. J. 1983. Fracture behavior of polymers. Applied Science Publishers. New York. 74-106 pp.

Roark, J. R. 2002. Formulas for stress and strain. 7th ed. McGraw-Hill, New York 28-50 pp.

CHAPTER 4. CONCLUSIONS

To analyze the fracture behavior of WPC, both experimental test and numerical method were employed. The density test results indicate that WPC made by the extrusion method had density variation in fiber orientation. The mean mass attenuation coefficient of WPC in the machine direction was 6% lower than that of WPC in the cross machine direction. The results of the impact test and three point bending test showed that compared to machine direction of WPC having the lower density value, cross machine direction having higher density value had better performance in those mechanical tests. Also as shown by the analysis of variance (ANOVA) and Tukey's test, the effect of stress concentration factor (S.C.F) and fiber orientation and combing effect on impact strength of WPC was significant. From the experimental test, it can be realized that fiber orientation was a key parameter on mechanical properties of WPC. Fracture surface examined by SEM show that impact specimen (machine direction) has fewer voids and smooth surface compared to impact specimen (cross machine direction). Fiber pullout due to impact energy occurred more frequently in impact specimen of machine direction while fiber breakage happened more frequently in impact specimen of cross machine direction. Therefore, the material used in this study had weak bondage between polymer and fibers.

The results of the four point bending test showed that notch length was an inverse function of modulus of rupture and peak load. Fracture toughness of WPC was evaluated as 1.79 (MPa$\sqrt{m}$). The result of this exploratory investigation indicates that there are inherent difficulties in using fracture toughness testing to determine the fracture

properties of fiber reinforced polymer. This is due to the very nature of complex matrices, the presence of fibers and the failure behavior of the composite, which are dependant on reinforcing parameters such as portion of fibers, polymers, porous, direction of fibers, and interfacial area. There are increasing needs to identify the most appropriate method to evaluate the fracture toughness of WPC.

A generalized analysis of local fitting methods for stress intensity factor determination using finite element method has been outlined. A discussion of the verification of the simulation was also shown. While fracture toughness of WPC is independent of notch length, stress intensity factor was a function of crack length.

The methodology used in this study suggests models to evaluate the impact strength and fracture toughness of WPC. It can also be used to develop more advanced models considering nonlinear fracture behavior to predict more accurately the mechanical and physical properties of WPC in future research.

APPENDIX A : STATISTIC ANALYSIS ON IMPACT STRENGTH OF WOOD PLASTIC COMPOSITE (WPC)

A.1 Statistic Analysis for Impact Strength Test of WPC

A.1.1 SAS Code for TWO-WAY ANOVA

```
data one;
input scf dir is;
datalines;
1 1 36.942
1 1 44.752
1 1 57.641
1 1 39.253
1 1 36.733
1 2 88.138
1 2 77.733
1 2 74.107
1 2 85.687
1 2 82.95
5 1 28.76
5 1 37.476
5 1 39.747
5 1 29.721
5 1 33.063
5 2 52.407
5 2 48.721
5 2 55.058
5 2 50.016
5 2 52.325
6.66 1 34.519
6.66 1 27.827
6.66 1 30.394
6.66 1 33.193
6.66 1 27.72
6.66 2 49.881
```

```
6.66 2 41.307
6.66 2 42.5
6.66 2 48.451
6.66 2 43.628
8.26 1 28.085
8.26 1 23.912
8.26 1 21.452
8.26 1 26.931
8.26 1 25.994
8.26 2 34.328
8.26 2 35.172
8.26 2 45.753
8.26 2 31.947
8.26 2 35.829
9 1 24.468
9 1 31.966
9 1 25.624
9 1 22.586
9 1 24.166
9 2 32.773
9 2 40.865
9 2 35.986
9 2 36.358
9 2 35.266
9.94 1 17.434
9.94 1 20.318
9.94 1 21.837
9.94 1 20.844
9.94 1 23.858
9.94 2 35.583
9.94 2 32.626
9.94 2 27.5
;
proc glm;
class scf dir;
```

```
model is=scf|dir;
lsmeans scf|dir/pdiff stderr adjust=tukey out=output;
output out=two p=yhat r=r;
run;
proc univariate data=two normal plot;
var r;
run;
proc gplot data=two;
plot r*yhat;
run;
proc mixed data=one;
class scf dir;
model is=scf|dir/htype=6 outp=SIX;
lsmeans scf|dir/pdiff adjust=tukey;
run;
quit;
```

Table A.6.1 A two-way ANOVA (analysis of variance) for impact strength of WPC

Source	DF	Sum of Square	Mean Square	F	Pr>F
Model	11	14363.771	1305.797	64.31	<.0001
Error	46	2373.501	20.304		
Corrected Total	57	15297.759			

R-Square	Coeff Var	Root MSE	Mean(IS)
0.938	11.614	4.506	38.795

Source	DF	Type I SS	Mean Square	F	Pr>F
scf	5	8477.106	1695.421	83.50	<.0001
dir	1	4447.152	4447.152	219.03	<.0001
scf*dir	5	1439.513		14.18	<.0001

Source	DF	Type III SS	Mean Square	F	Pr>F
scf	5	8105.392	1621.078	79.84	<.0001
dir	1	4261.021	4261.021	209.86	<.0001
scf*dir	5	1439.513	287.902	14.18	<.0001

Table A.6.2 The results of difference of impact strength of WPC based on the effect of stress concentration factor and fiber orientation (Tukey's test)

Effect	scf	dir	_scf	_dir	Estimate	S.T.D	DF	t Value	Pr>|t|	Adjustment
scf	1		6.66		24.4516	2.0151	46	12.13	<.0001	Tukey
scf	1		8.26		31.4533	2.0151	46	15.61	<.0001	Tukey
scf	1		9		31.3878	2.0151	46	15.58	<.0001	Tukey
scf	1		9.94		36.0130	2.1766	46	16.55	<.0001	Tukey
scf	5		6.66		4.7874	2.0151	46	2.38	0.0217	Tukey
scf	5		8.26		11.7891	2.1766	46	5.85	<.0001	Tukey
scf	5		9		11.7236	2.0151	46	5.82	<.0001	Tukey
scf	5		9.94		16.3488	2.0151	46	7.51	<.0001	Tukey
scf	6.66		8.26		7.0017	2.1766	46	3.47	0.0011	Tukey

(Table continue)

scf	6.66		9		6.9362	2.0151	46	3.44	0.0012	Tukey
scf	6.66		9.94		11.5614	2.1766	46	5.31	<.0001	Tukey
scf	8.26		9		-0.0655	2.0151	46	-0.03	0.9742	Tukey
scf	8.26		9.94		4.5597	2.1766	46	2.09	0.0417	Tukey
scf	9		9.94		4.6252	2.1766	46	2.12	0.0390	Tukey
dir		1		2	-17.316	1.1953	46	-14.4	<.0001	Tukey
scf*dir	1	1	1	2	-38.658	2.8498	46	-13.5	<.0001	Tukey
scf*dir	1	1	5	1	9.3108	2.8498	46	3.27	0.0021	Tukey
scf*dir	1	1	5	2	-8.6412	2.8498	46	-3.03	0.0040	Tukey
scf*dir	1	1	6.66	1	12.3336	2.8498	46	4.33	<.0001	Tukey
scf*dir	1	1	6.66	2	-2.0892	2.8498	46	-0.73	0.4672	Tukey
scf*dir	1	1	8.26	1	17.7894	2.8498	46	6.24	<.0001	Tukey
scf*dir	1	1	8.26	2	6.4584	2.8498	46	2.27	0.0282	Tukey
scf*dir	1	1	9	1	17.3022	2.8498	46	6.07	<.0001	Tukey
scf*dir	1	1	9	2	6.8146	2.8498	46	2.39	0.0209	Tukey
scf*dir	1	1	9.94	1	22.2060	2.8498	46	7.79	<.0001	Tukey
scf*dir	1	1	9.94	2	11.1612	3.2097	46	3.39	0.0014	Tukey
scf*dir	1	2	5	1	47.9696	2.8498	46	16.83	<.0001	Tukey
scf*dir	1	2	5	2	30.0176	2.8498	46	10.53	<.0001	Tukey
scf*dir	1	2	6.66	1	50.9924	2.8498	46	17.89	<.0001	Tukey
scf*dir	1	2	6.66	2	36.5696	2.8498	46	12.83	<.0001	Tukey
scf*dir	1	2	8.26	1	56.4482	2.8498	46	19.81	<.0001	Tukey
scf*dir	1	2	8.26	2	45.1172	2.8498	46	15.83	<.0001	Tukey
scf*dir	1	2	9	1	55.9610	2.8498	46	19.64	<.0001	Tukey
scf*dir	1	2	9	2	45.4734	2.8498	46	15.96	<.0001	Tukey
scf*dir	1	2	9.94	1	60.8648	2.8498	46	21.36	<.0001	Tukey
scf*dir	1	2	9.94	2	49.8200	3.2907	46	15.14	<.0001	Tukey
scf*dir	5	1	5	2	-17.952	2.8498	46	-6.30	<.0001	Tukey
scf*dir	5	1	6.66	1	3.0228	2.8498	46	1.06	0.2944	Tukey
scf*dir	5	1	6.66	2	-11.400	2.8498	46	-4.00	0.0002	Tukey
scf*dir	5	1	8.26	1	8.4786	2.8498	46	2.98	0.0047	Tukey
scf*dir	5	1	8.26	2	-2.8524	2.8498	46	-1.00	0.3221	Tukey
scf*dir	5	1	9	1	7.9914	2.8498	46	2.80	0.0074	Tukey
scf*dir	5	1	9	2	-2.4962	2.8498	46	-0.88	0.3856	Tukey

(Table continue)

scf*dir	5	1	9.94	1	12.8952	2.8498	46	4.52	<.0001	Tukey
scf*dir	5	1	9.94	2	1.8504	3.2097	46	0.56	0.5766	Tukey
scf*dir	5	2	6.66	1	20.9748	2.8498	46	7.36	<.0001	Tukey
scf*dir	5	2	6.66	2	6.5520	2.8498	46	2.30	0.0261	Tukey
scf*dir	5	2	8.26	1	26.4306	2.8498	46	9.27	<.0001	Tukey
scf*dir	5	2	8.26	2	15.0996	2.8498	46	5.30	<.0001	Tukey
scf*dir	5	2	9	1	25.9434	2.8498	46	9.10	<.0001	Tukey
scf*dir	5	2	9	2	15.4558	2.8498	46	5.42	<.0001	Tukey
scf*dir	5	2	9.94	1	30.8472	2.8498	46	10.82	<.0001	Tukey
scf*dir	5	2	9.94	2	19.8024	3.2907	46	6.02	<.0001	Tukey
scf*dir	6.66	1	6.66	2	-14.422	2.8498	46	-5.06	<.0001	Tukey
scf*dir	6.66	1	8.26	1	5.4558	2.8498	46	1.91	0.0618	Tukey
scf*dir	6.66	1	8.26	2	-5.8752	2.8498	46	-2.06	0.0449	Tukey
scf*dir	6.66	1	9	1	4.9686	2.8498	46	1.74	0.0879	Tukey
scf*dir	6.66	1	9	2	-5.5190	2.8498	46	-1.94	0.0590	Tukey
scf*dir	6.66	1	9.94	1	9.8724	2.8498	46	3.46	0.0012	Tukey
scf*dir	6.66	1	9.94	2	-1.1724	3.2907	46	-0.36	0.7233	Tukey
scf*dir	6.66	2	8.26	1	19.8786	2.8498	46	6.98	<.0001	Tukey
scf*dir	6.66	2	8.26	2	8.5476	2.8498	46	3.00	0.0044	Tukey
scf*dir	6.66	2	9	1	19.3914	2.8498	46	6.80	<.0001	Tukey
scf*dir	6.66	2	9	2	8.9038	2.8498	46	3.12	0.0031	Tukey
scf*dir	6.66	2	9.94	1	24.2952	2.8498	46	8.53	<.0001	Tukey
scf*dir	6.66	2	9.94	2	13.2504	3.2907	46	4.03	0.0002	Tukey
scf*dir	8.26	1	8.26	2	-11.331	2.8498	46	-3.98	0.0002	Tukey
scf*dir	8.26	1	9	1	-0.4872	2.8498	46	-0.17	0.8650	Tukey
scf*dir	8.26	1	9	2	-10.974	2.8498	46	-3.85	0.0004	Tukey
scf*dir	8.26	1	9.94	1	4.4166	2.8498	46	1.55	0.1281	Tukey
scf*dir	8.26	1	9.94	2	-6.6282	3.2907	46	-2.01	0.0499	Tukey
scf*dir	8.26	2	9	1	10.8438	2.8498	46	3.81	0.0004	Tukey
scf*dir	8.26	2	9	2	0.3562	2.8498	46	0.12	0.9011	Tukey
scf*dir	8.26	2	9.94	1	15.7476	2.8498	46	5.53	<.0001	Tukey
scf*dir	8.26	2	9.94	2	4.7028	3.2907	46	1.43	0.1597	Tukey
scf*dir	9	1	9	2	-10.487	2.8498	46	-3.68	0.0006	Tukey
scf*dir	9	1	9.94	1	4.9038	2.8498	46	1.72	0.0920	Tukey

(Table continue)

scf*dir	9	1	9.94	2	-6.1410	3.2907	46	-1.87	0.0684	Tukey
scf*dir	9	2	9.94	1	15.3914	2.8498	46	5.40	<.0001	Tukey
scf*dir	9	2	9.94	2	4.3466	3.2907	46	1.32	0.1931	Tukey
scf*dir	9.94	1	9.94	2	-11.044	3.2907	46	-3.36	0.0016	Tukey

APPENDIX B : FINITE ELEMENT ANALYSIS ON FRACTURE BEHAVIOR OF WOOD PLASTIC COMPOSITE (WPC)

B.1 Finite Element Analysis

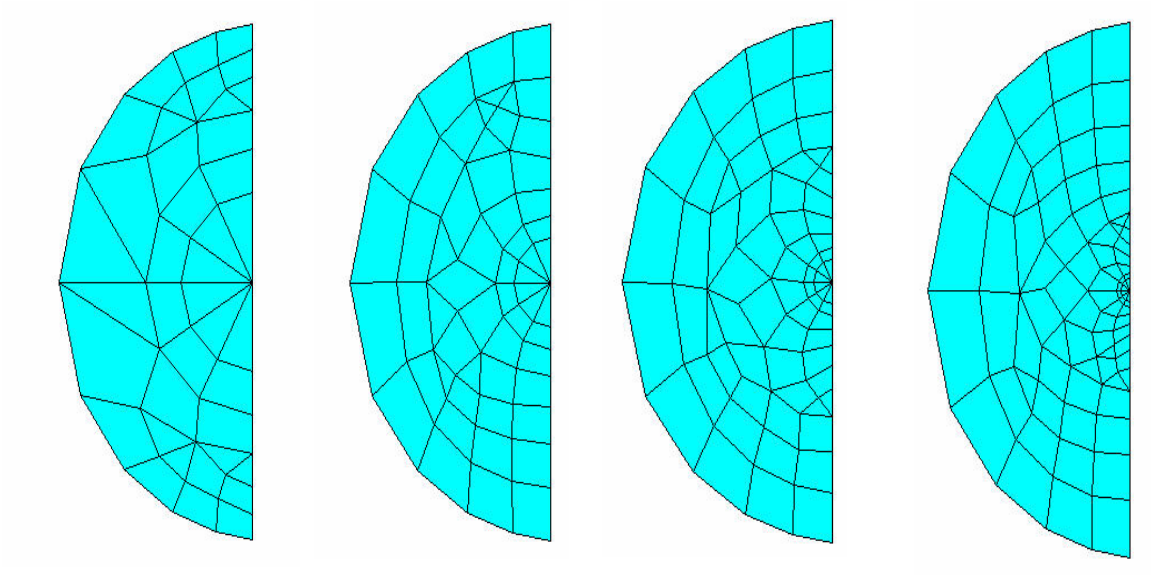

Figure B.2. The sequence of four meshes around the crack tip.

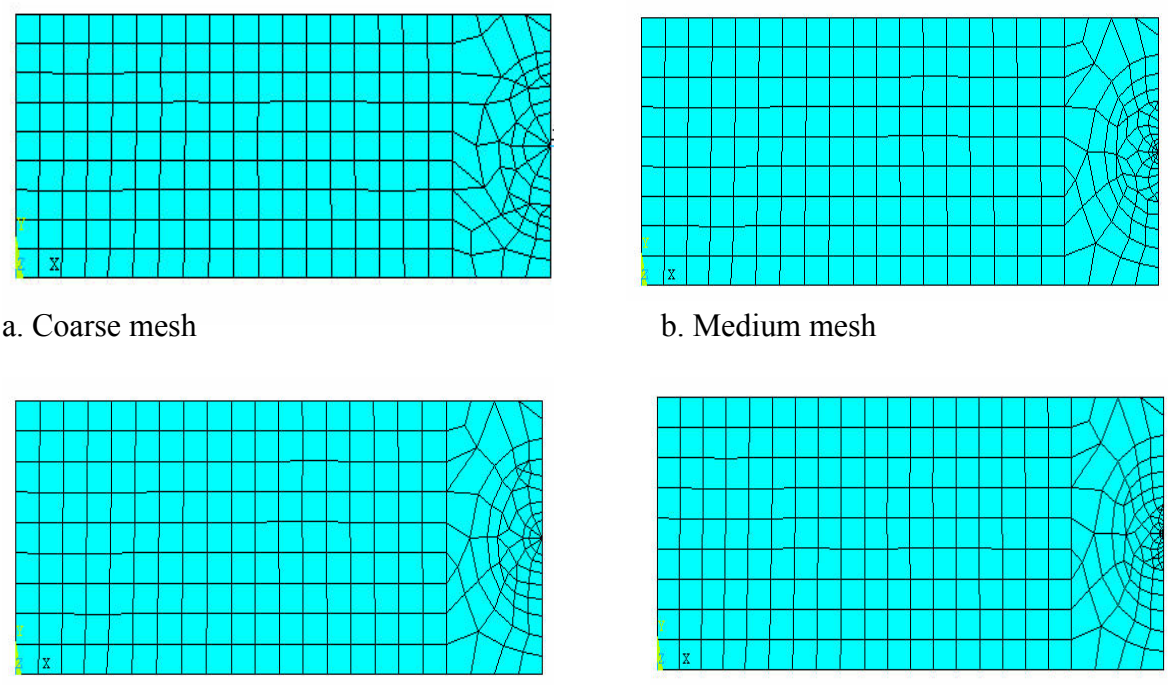

a. Coarse mesh

b. Medium mesh

c. Fine mesh

d. Super Fine mesh

Figure B.3. The sequence of four meshes for four point bending simulation.

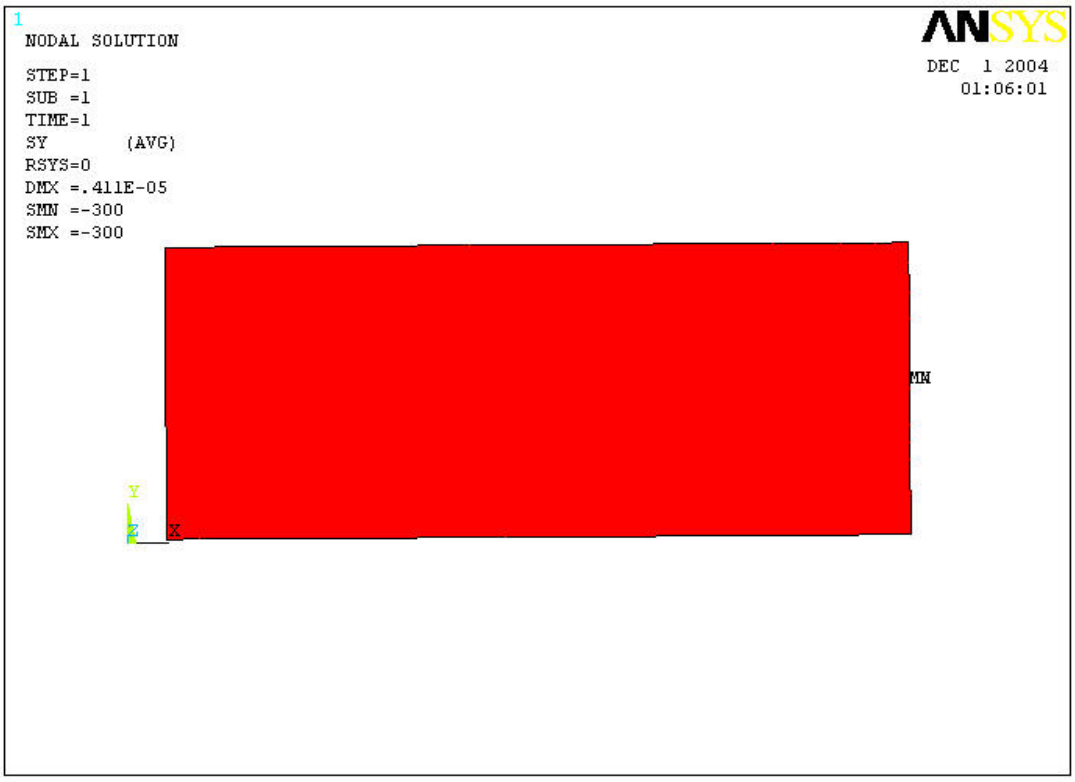

Figure B.5. Patch test to check connectivity of each element

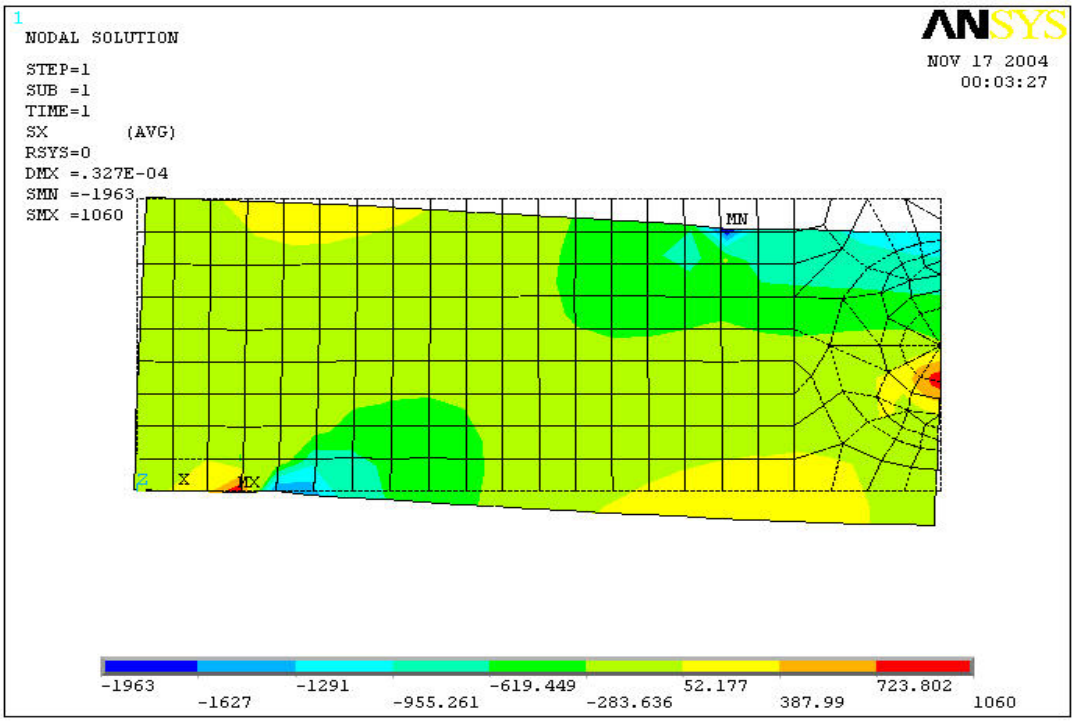

Figure B.6. Contour plot of the normal stress(σ_x) on coarse grid

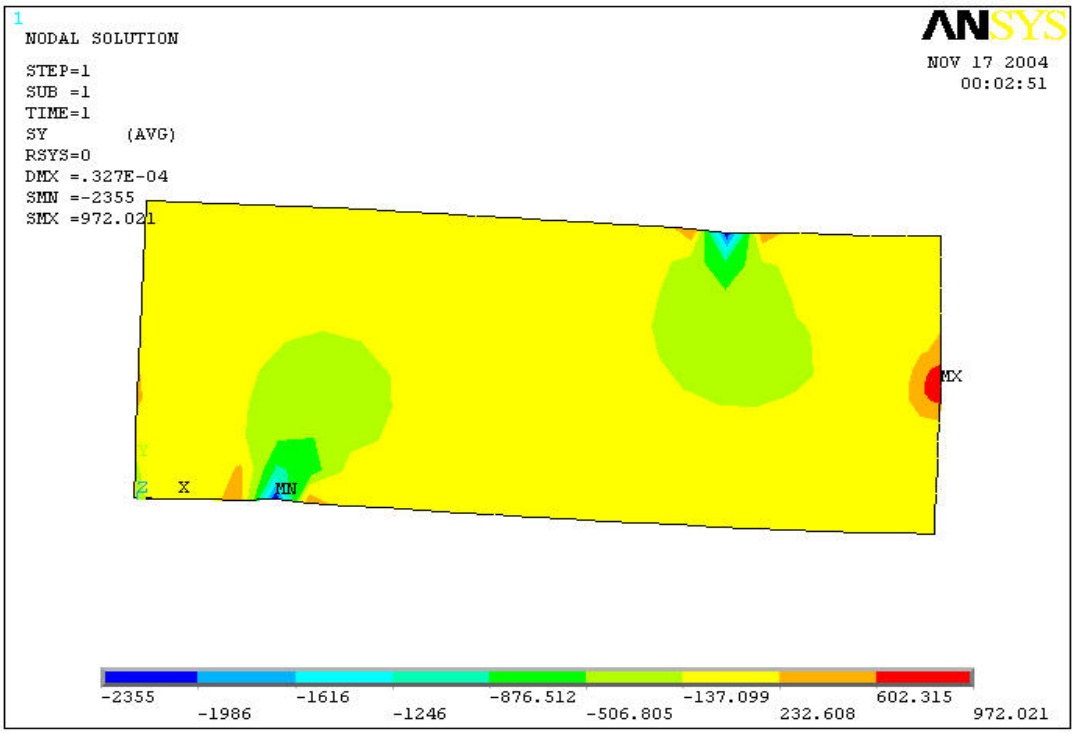

Figure B.7. Contour plot of the normal stress(σ_y) on coarse grid

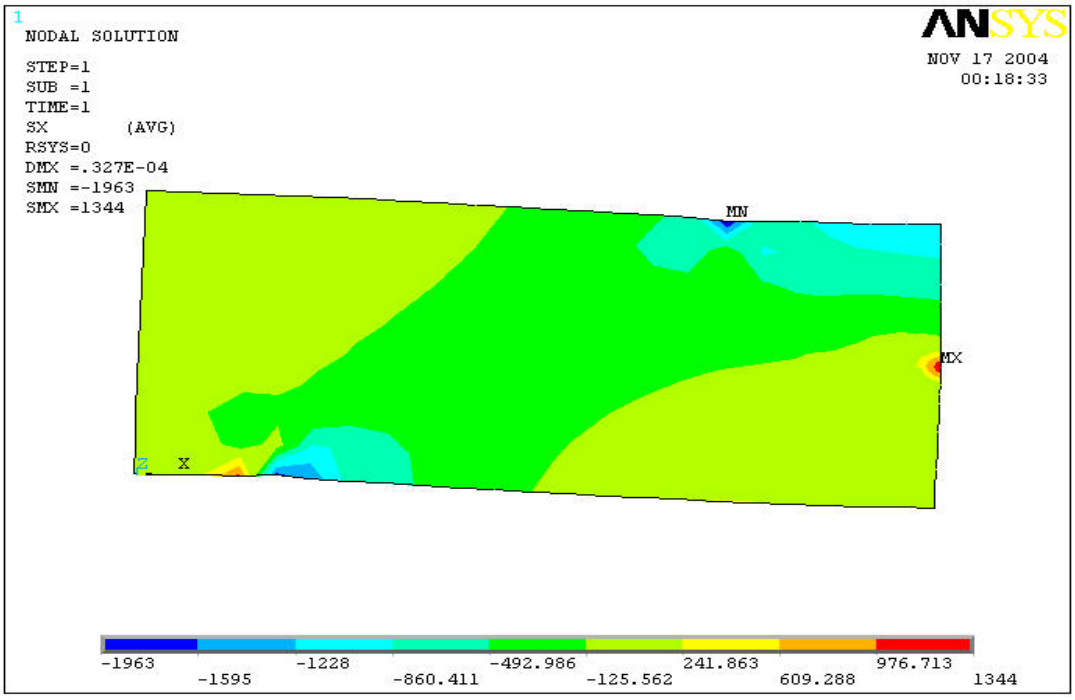

Figure B.8. Contour plot of the normal stress(σ_x) on medium grid

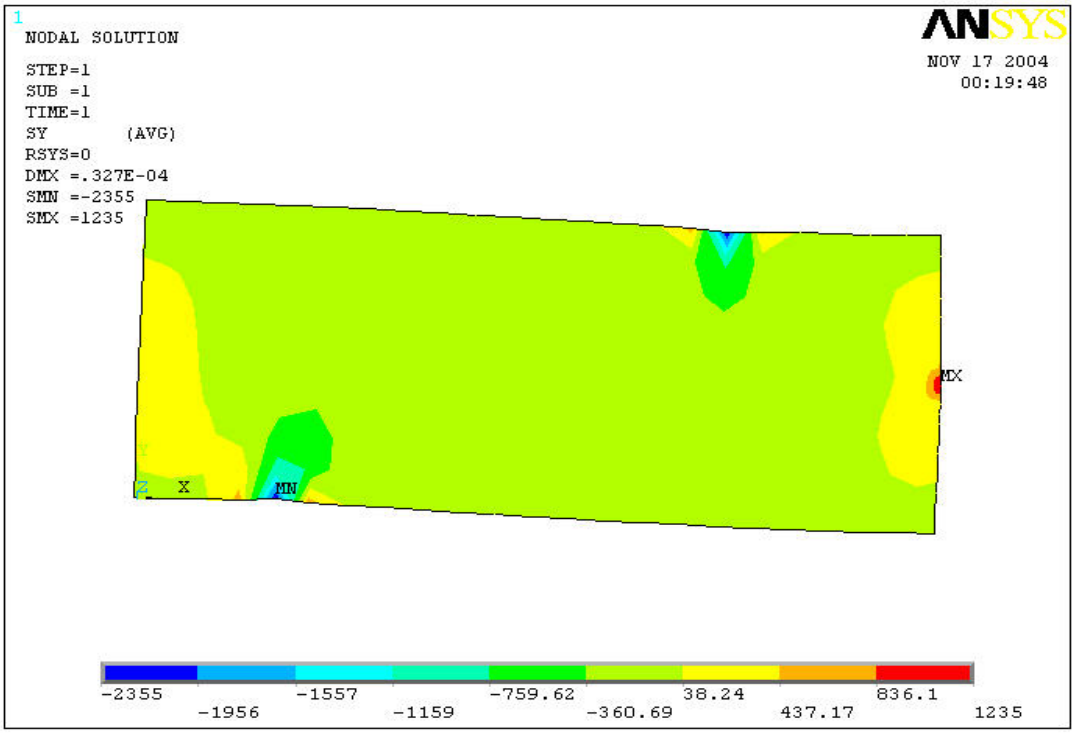

Figure B.9. Contour plot of the normal stress(σ_y) on medium grid

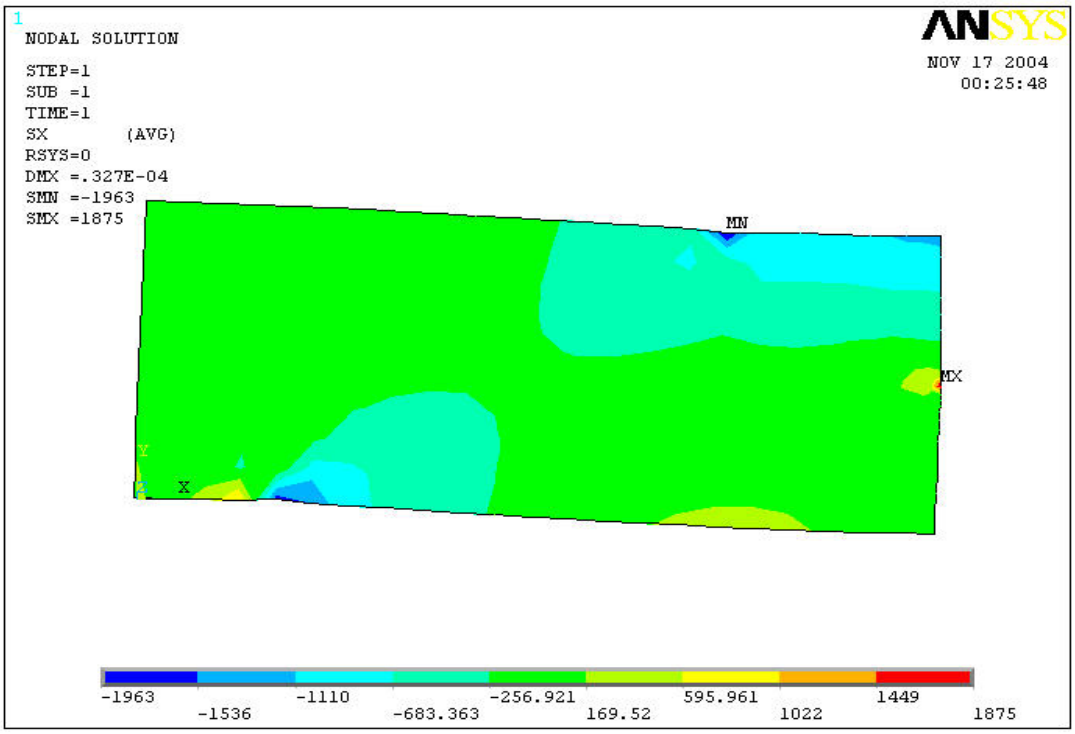

Figure B.10. Contour plot of the normal stress(σ_x) on fine grid

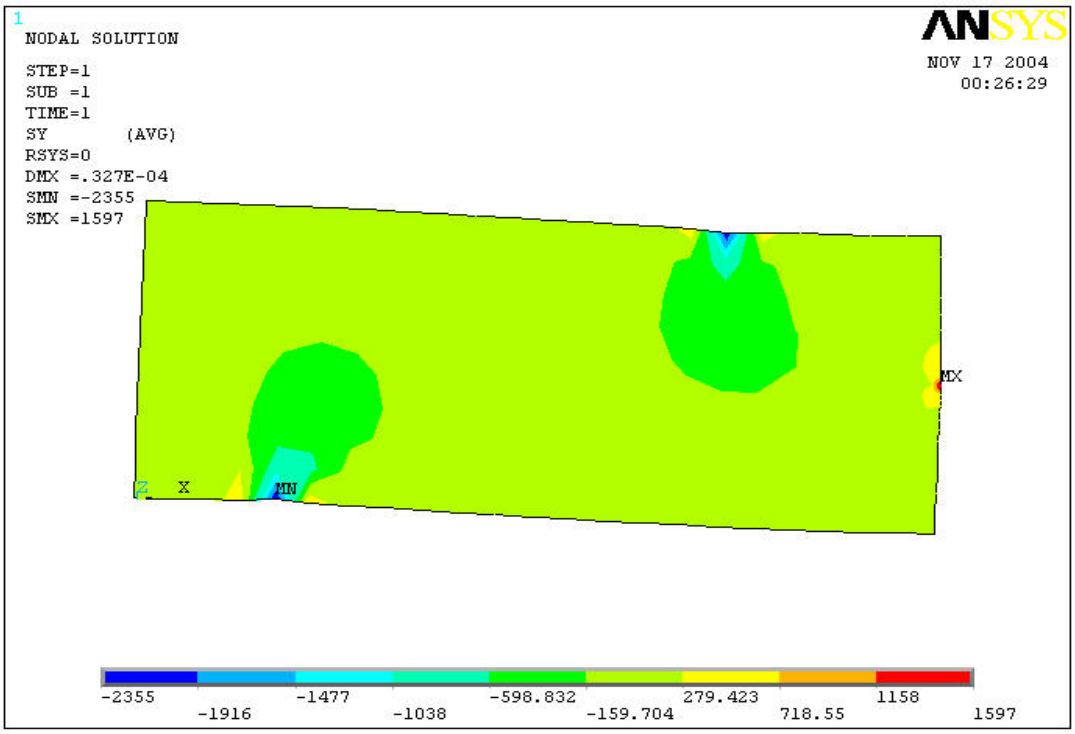

Figure B.11. Contour plot of the normal stress(σ_y) on fine grid

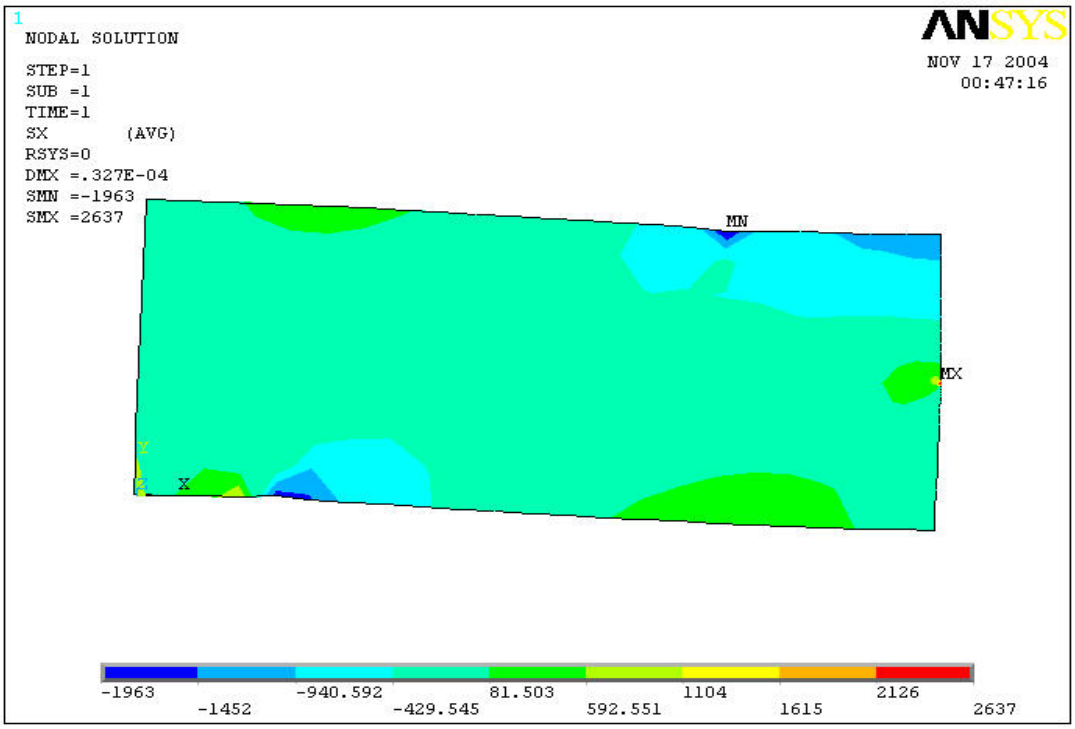

Figure B.12. Contour plot of the normal stress(σ_x) on super fine grid

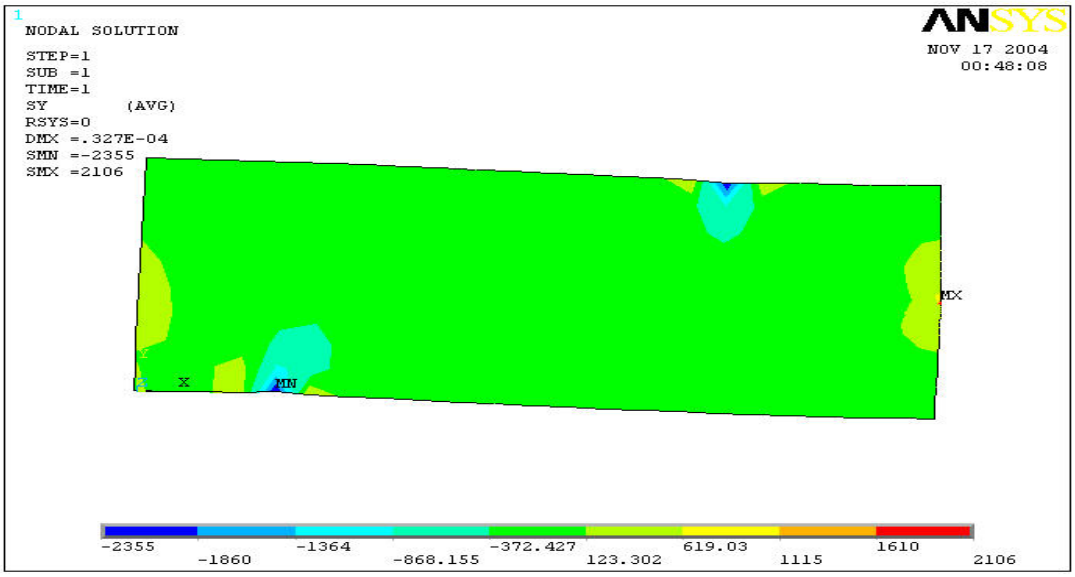

Figure B.13. Contour plot of the normal stress(σ_y) on super fine grid

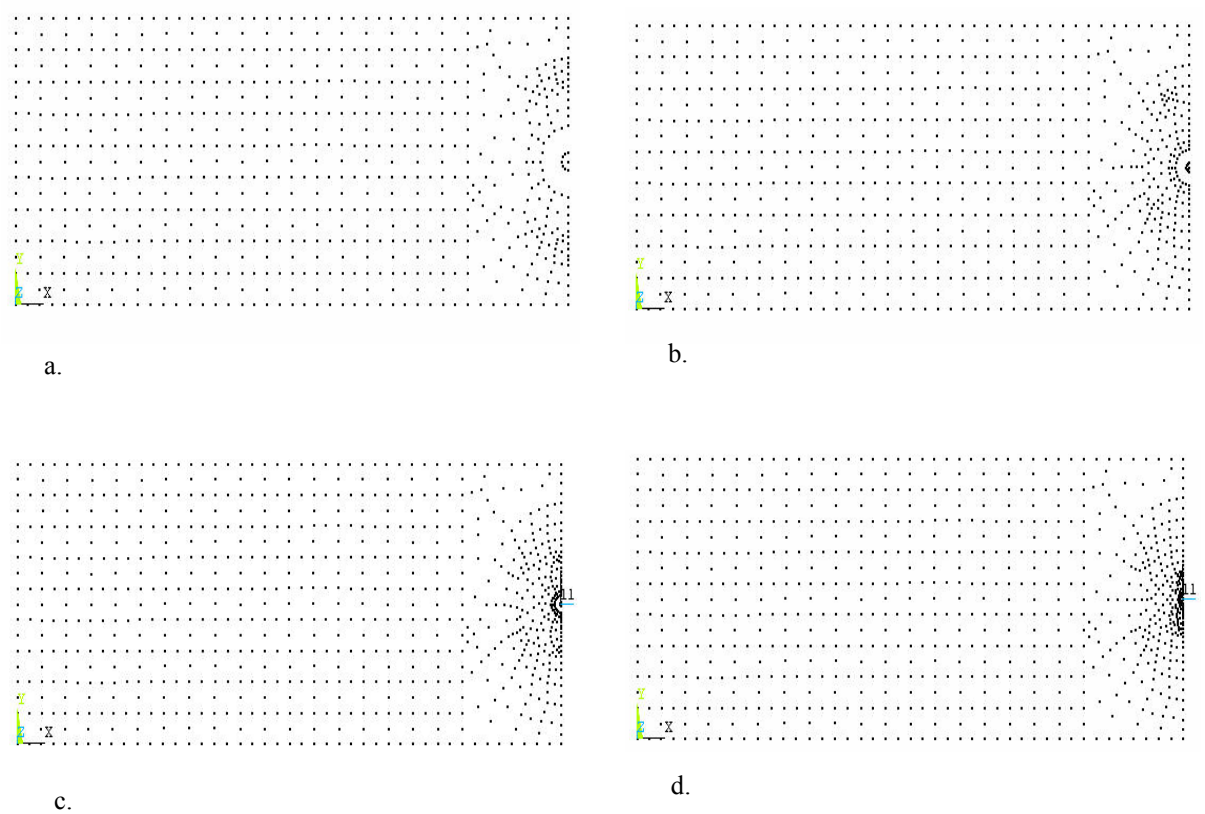

a. b.

c. d.

Figure B.14. Node plot of the sequence of four grids. coarse grid node (a), medium grid node (b), fine gride node (c), and super fine grid (d)

VITA

Gi Young Jeong was born on December 23, 1978, in Gwang-ju, Korea, to parents Byung Hoo and Bong Sim. Gi Young resided in his home town until he graduated from Chonnam National University with a bachelor's degree from the Wood Science and Engineering Department in May 2004. During his undergraduate studies, he joined the army in 1998. He served in the demilitarized zone (DMZ) in Cholwon, which is the closest to North Korea. His military experience enhanced his working behavior and gave him a strong body and mind. After discharge from the army in 2000, he continued his education while working as a research assistant in the wood physics lab in Chonnam National University. He was involved in many projects regarding wood composites. He developed a basic knowledge on wood composites and decided to study abroad to learn advanced knowledge and technology on wood based composite. In 2004 he joined Louisiana State University (LSU) in pursuit of a Master of Science degree in forestry. During his master courses, he worked as an executive member in Korean student association at LSU. He will receive the degree of Master of Science at the August commencement in 2005. He will pursue doctorial studies at the Department of Wood Science and Engineering in Oregon State University from September 2005.